CHARACTERIZING THE TOPOLOGY OF PARTIALLY POLARIZED VORTEX BEAMS

by

William Scott Raburn

A dissertation submitted to the faculty of
The University of North Carolina at Charlotte
in partial fulfillment of the requirements
for the degree of Doctor of Philosophy in
Optical Science and Engineering

Charlotte

2024

Approved by:

_____
Dr. Greg Gbur

_____
Dr. Angela Allen

_____
Dr. Tsing-Hua Her

_____
Dr. Charles Lee

ABSTRACT

WILLIAM SCOTT RABURN. Characterizing the Topology of Partially Polarized Vortex Beams. (Under the direction of DR. GREG GBUR)

Singularities defining the topology for the polarization state of nonuniformly polarized electromagnetic beams have been a topic of both theoretical and practical interest, including improvements to remote sensing and free-space optical communications, for many years. However, atmospheric turbulence can distort the features of singularities over long propagation distances, limiting their use in many cases. One solution being considered is the reduction of spatial coherence of light, as partially coherent beams have shown increased resistance to turbulence under a broad range of situations. Work on coherence singularities of scalar fields supports this as well. However there has been relatively little work done to explore singularities of the intersection of the two phenomena of nonuniform partial coherence and nonuniformly polarized fields. Namely the singularities in the unified representation of coherence and polarization state, such as the cross spectral density matrix of nonuniformly partially polarized wavefields.

In this dissertation, we use a simple model of partially polarized electromagnetic vortex beams to highlight three different ways that one can define polarization singularities in scalar wavefields. One of those, projections of the cross spectral density matrix defining the beam, has not previously been discussed. We then detail the evolution of those novel partial polarization singularities and how the position and number of singularities are affected by different levels of atmospheric turbulence. We find that there are projections where the singularities persist on propagation, suggesting their possible use in applications.

We lastly explore a potentially simpler way to express polarization and partial polarization singularities as phase singularities. It was established by Green and

Wolf in 1953 that an electromagnetic wave can be characterized by a complex scalar potential, including its energy and momentum densities. In this paper, we show that for electromagnetic beams this scalar potential can be used to fully describe the beam's topology. We further demonstrate that this scalar potential can be used to characterize the topology of partially polarized vector beams as well.

ACKNOWLEDGEMENTS

I would like to acknowledge my advisor Dr. Greg Gbur whose guidance and collaboration made this work possible.

TABLE OF CONTENTS

LIST OF FIGURES viii

CHAPTER 1: SINGULARITIES OF PARTIALLY POLARIZED VORTEX BEAMS 7

1.1. Introduction 7

1.2. Polarization singularities 9

1.3. Partial coherence in scalar and vector fields 12

1.4. Singularities in partially coherent vector beams 15

1.5. Construction of model PC beams 19

1.6. Singularities in model beams 24

1.7. Conclusion 28

CHAPTER 2: EVOLUTION OF THE POLARIZATION SINGULARITIES IN PARTIALLY COHERENT BEAMS ON PROPAGATION THROUGH TURBULENCE 31

2.1. Introduction 31

2.2. Characterizing partially coherent vector beams and their singularities 33

2.3. Model of partially polarized vector vortex beam 37

2.4. Propagation of the model 44

2.5. Topological changes with propagation 47

2.5.1. Stable projections 48

2.5.2. Initial coherence interplay with turbulence effects 51

2.5.3. Projections Topology As cross Section of Topology in $(\boldsymbol{p}, \boldsymbol{q}, z)$ 53

2.6. Conclusion 55

CHAPTER 3: A SCALAR POTENTIAL FOR REPRESENTING THE TOPOLOGY OF ELECTROMAGNETIC BEAMS 57

3.1. Introduction 57

3.2. The Green-Wolf scalar representation 59

3.3. Monochromatic beams and their singularities 61

3.4. Physical properties of the complex scalar 66

3.5. Stokes-like parameters for describing singularities 68

3.6. Extension to partially polarized vector beams 70

3.7. Dynamic topology of V along L lines 73

3.8. Conclusions 75

REFERENCES 82

LIST OF FIGURES

FIGURE 1: Polarization Ellipse 4

FIGURE 1.1: lemon and star C-points 10

FIGURE 1.2: singularity in $\bar{\mathbf{J}}$ 25

FIGURE 1.3: singularities in eta of beam with $t_R = 1$, $t_L = 0$ 26

FIGURE 1.4: Singularities in eta of beam with $t_R = 2$, $t_L = 1$ 27

FIGURE 1.5: Singularities of projection onto the polarized part at the reference point for beam with $t_R = 1$, $t_L = 0$ 27

FIGURE 1.6: Singularities of projection onto the polarization perpendicular to the polarized part at the reference point for beam with $t_R = 1$, $t_L = 0$ 28

FIGURE 1.7: Singularities of projection for beam with $t_R = 2$, $t_L = 1$ 29

FIGURE 2.1: Changes in singularity position with changes to the polarization projected onto 43

FIGURE 2.2: Example of a stable trajectory of singularities on propagation. 49

FIGURE 2.3: Singularities evolution for initially coherent beam propagated through moderate turbulence 50

FIGURE 2.4: turbulence levels affect on movement of extra singularities form partial coherence toward and away from the beam center on propagation 51

FIGURE 2.5: Changes in visibility of singularities with changes in projection coordinate and polarization shape 53

FIGURE 2.6: Using multiple projections for understanding of higher dimensional structure of the singularity 55

FIGURE 3.1: equivalence of phase and angle of major axis of polarization 66

INTRODUCTION

This dissertation expands the field of singular optics to cover the topology of nonuniformly partially polarized vortex fields. These are beams where the polarization is nonuniform within the cross section and the degree of polarization varies as well.

Singular optics is the field of research concerned with singularities in attributes of fields used to describe electromagnetic waves, and the associated topology. For most of the history of optics research the emphasis has been on where electro-magnetic field has higher intensity, however after researchers began noting the topology of the fields phase near where the intensity is zero more research was done in this direction creating the subfield of singular optics. Singular optics as a field is the study discontinuities in some aspect of any category of oscillating electromagnetic fields. This dissertation explores singular optics in electromagnetic beams specifically. The simplest type of singularity is in the phase when fields can be treated as scalars.

For electromagnetic fields whether the full vector description is used or it is treated as a scalar, the electric field as an observable is real valued. Despite this the complex field $\tilde{U}(\boldsymbol{r},t)$ is often used for convenience in place of

$$U(\boldsymbol{r},t) = \tilde{U}(\boldsymbol{r},t) + \tilde{U}^*(\boldsymbol{r},t)\ . \tag{1}$$

where for monochromatic fields $\tilde{U}(\boldsymbol{r},t) = \tilde{U}(\boldsymbol{r})e^{-i\omega t}$. The phase of a scalar field, or component of a vector field, then becomes the argument of the complex field making it much more tractable analytically and often for the monochromatic fields used in this dissertation the complex value $\tilde{U}(\boldsymbol{r})$ will be used, without the tilde, in place of

the real valued scalar or vector field. While many may consider this form merely a mathematical convenience they are also the field values that follow from the complex valued electromagnetic 4-potential used in quantum electrodynamics. This singularity occurs at locations where the intensity is zero. For instance the a phase singularity is present along the $\hat{z}$ axis of any field

$$U(x, y, z) = (x \pm iy)^m u(x, y, z) \tag{2}$$

where $m \geq 0$ is an integer and u is defined at the axis where $U(0, 0, z) = 0$ and the intensity, $U^(\boldsymbol{r}) * U(\boldsymbol{r})$, is zero. At that point $\mathrm{Arg}(U)$ the phase is undefined with the a value in the neighborhood of the point changing by an integer multiple of 2π as the point is circled. These singularities and the space around it make up what are called optical vortices due to how the phase dependence on the optical axis, z, and time cause this phase change with the azimuthal angle to take the form of rotating with respect to both in a manner reminiscent of a vortex. These vortices and the singularities they surround have found application in fields like free-space communication, optical tweezing, and imaging processing.

Singular optics includes the study of singularities in many other aspects of fields, whose locations while associated the zeros of some variable are not necessarily at zeros of intensity. Most singularities share the structure of a singular point in the cross section of a beam around which the property that is undefined at the point changes as the point is circled returning to the same or equivalent value due to the property being a phase or physical angle. In those cases interesting 'new physics' come with introduction of integer valued topological charges, for phase, and indices for others to describe the singularity. The total charge or index of the beam is conserved, leading to the singularities acting similarly to pseudo-particles being created and destroyed in opposite pairs or decaying from a singularity with a higher topological charge

to multiple lower charge singularities, meaning there is new physics to explore with every new type. There are still many types of singularities that either haven't been studied extensively or haven't been defined at all and this dissertation will explore these singularities.

The type of beams that have had their singularities and topology studied more than any other, aside from scalar beams, are electromagnetic beams. These are beams where the scalar approximation is no longer applicable and the state of polarization is not uniform along a beam cross section. In these beams it is the orientation of the polarization ellipse and handedness that can have singularities rather than the phase since each of the two components of the field have their own independent phase.

Polarization singularities are more complex then phase singularities or even simply in singularities in the angle of a real vector field as can be seen in figure 1 of the polarization ellipse, a shape used to physically describe polarization, where there is orientation, shape and handedness. Isolated points of circular polarization in the cross section of a beam, called C-points, are singularities in the orientation of the polarization ellipse, while isolated lines of linear polarization called L-lines are singularities in the handedness of the polarization. Less typically a singularity in both can exist and these are known as V-points. Like the phase singularities these polarization singularities have found use in free-space communication among other applications.

This pattern of a change in the beam, in this case from uniformly polarized to nonuniformly polarized causing the singularity types present to change, is common pattern. A beam can also lack a phase singularity when the overall coherence of a beam decreases. When even simply two monochromatic beams of close frequency interact they produce a beat effect if the frequency bandwidth of a beam of light can not be ignored the modes at different frequencies similarly add to each other with seemingly random phase difference leading to the random value of the field. This random fluctuation whether it is caused by randomness in the source medium or just

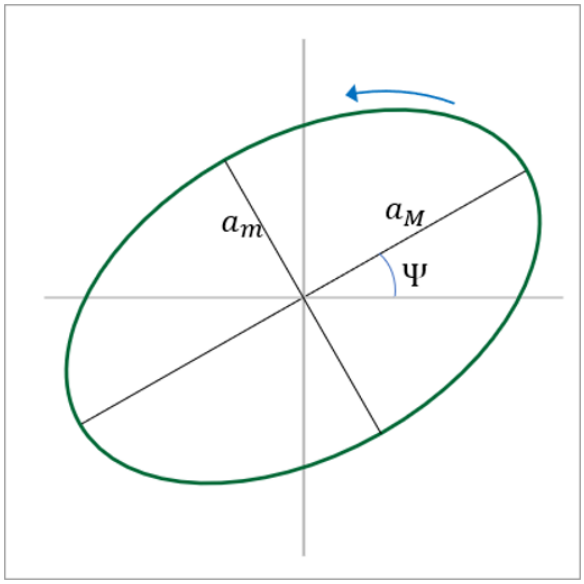

Figure 1: Above is pictured a generic polarization ellipse. It shows the path that the electric field $\boldsymbol{E}(\boldsymbol{r}, t)$ would trace out over time if the tail of its vector is at the origin. The orientation of the ellipse is defined by the angle Ψ between the major axis where $|\boldsymbol{E}| = a_M$ and the x axis.

the beam frequency width causes the zeros in intensity to be 'washed out' by the random fluctuations that come with decreased coherence. The study of singularities of partially coherent vortices began more recently but is becoming well established. Instead of singularities in the field itself, singularities exist in the phase of the cross spectral density between two points. The phase singularities of this complex scalar even just within a cross section of the beam are embedded in a four dimensional space of the two points. This too has been suggested for use in free-space communication since beams traveling through turbulent air will naturally lose some coherence.

Due to the relatively young age of singular optics there are many types of optical singularities that have yet to be fully explored or even defined. There are many types of singularities in optics whose physics are only just beginning to be explored, remain completely unexplored or even have yet to be identified. Some of these are more complex beams such as higher moments or multi-frequency beams as well as combinations of these characteristics with others such as partial coherence or nonuni-

form polarization. Each of these can also be further complicated by different media types that they could be propagating through. There are also other simple esoteric characterizations of a beam whose singularities may be found.

This dissertation attempts to expand the breadth of singularity types studied by defining novel singularities and creating a class of beams useful for exploring topologies associated with partially coherent nonuniformly polarized beams. The singularities explored represent in a way two ends of the spectrum of topological topics left to be explored.

The first involves singularities of beams with the combined properties of two types of beams for which singularities have already been studied by themselves, nonuniform polarization and partial coherence. As both have relevance to the same application of free space communication looking into a beam, with the advantages of both is desired. The topology of both introduce complications, as compared to phase singularities of coherent scalar fields, due to the matrix definition when considering nonuniform polarization and the need for a function of two points for nonuniform coherence. The cross-spectral density matrix used to describe such a beam therefore has a more complex topology then either the polarization matrix or the scalar cross spectral density.

The second description of the electromagnetic beam is unlike the first both of a very simple structure a complex scalar that is a function of position and time. This is the complex scalar potential that Green and Wolf defined, in 1953, that justifies the use of scalar waves in optics through its construction dependent on polarization of modes. Other than as a justification for using scalar wave descriptions in any case if one is only concerned with energy and momentum, the idea though novel never found much use on its own but may now find new use when applied to fields such as singular optics that did not exist at the time the idea was first introduced. We find that the phase singularities of the complex scalar potential have a meaning distinct

from that of a simple scalar beam and the polarization of a vector beam. However the time average of its square and other second order parameters fully reproduce the topology of the full vector beam just as Green and Wolf originally showed that the energy and momentum density could be found. Similarly the topology of partially polarized beams can also be found by expanding those same parameters to two points.

Like the more robustly studied topologies of singular optics the topologies associated with these novel singularity types will have interesting physics related to the interaction of singularities both in propagation and as the character of the beam changes. They also may prove useful for applications especially free-space communication.

The chapters of this dissertation consist of three papers that cover these topics. The first chapter explores three types of singularities that exist for partially polarized vortex beams, and introduces an appropriate class of beams to explore the form these singularities take in a cross section of the beam and how they relate to the fully polarized vector vortex beams. The second paper more fully describes the topology of one those types of singularities, the vector field given from projections of the cross spectral density matrix. This is done by analytically propagating our class of beam through different levels of turbulence and in the process creating a more general class of beams of partially polarized vortex beams as well.

Finally in the third paper we look at singularities of the complex scalar potential introduced by Green and Wolfe in the case of beams. Despite its scalar nature we are able to fully reproduce the topology of the polarization ellipse and this perspective gives us new insights and in some cases brings simplification when modeling the beam.

CHAPTER 1: SINGULARITIES OF PARTIALLY POLARIZED VORTEX BEAMS

abstract

Singularities in the polarization state of nonuniform electromagnetic beams have been a topic of both theoretical and practical interest for many years, as have singularities in the correlation functions of random scalar wavefields. However, there has been relatively little work done to explore the intersection of these phenomena, namely singularities in the polarization state of partially coherent wavefields. In this paper, we use a simple model of a partially coherent electromagnetic vortex beam to highlight three different ways that one can define polarization singularities in scalar wavefields, one of which has been not previously been discussed.

1.1 Introduction

The study and application of singularities in wavefields has grown in recent years into a vibrant and significant subfield of optics, known as singular optics [1, 2, 3]. The most commonly discussed types of such singularities are phase singularities in scalar waves, which typically manifest as lines of zero intensity in three-dimensional space. Around these singularities the phase has a circulating or helical structure, which has led to them being called *optical vortices*, here referred to as *scalar optical vortices*. Such singularities have been applied to fields such as free-space optical communication [4, 5], optical tweezing [6, 7] and image processing [8, 9].

To use a scalar wave description of light, the state of polarization is assumed to be uniform. Research over the past twenty years has demonstrated, however, that novel effects arise for optical beams that have spatially-varying polarization, known as *vector beams*. For vector beams, singularities of phase are no longer typical, and

instead the most common singularities are singularities of the state of polarization. These come in two generic types: C-points (points of circular polarization where the orientation of the polarization ellipse is undefined) and L-lines (lines of linear polarization where the helicity of the polarization ellipse is undefined). Much work has been done to elucidate the properties of polarization singularities, and beams with such singularities have been shown to be useful in a number of applications, including focusing [10, 11] and atmospheric propagation [12, 13].

But no light wave is truly monochromatic, and in recent years researchers have delved into the behavior of wavefield singularities when the field is partially coherent. For the scalar case, it has been shown that phase singularities evolve into singularities of the two-point correlation function when the spatial coherence of a wavefield is decreased [14, 15, 16]. There has now been a significant amount of research on partially coherent scalar vortex beams [17, 18, 19, 20].

In contrast, there has been relatively little work done to investigate the nature of polarization singularities in partially coherent vector vortex beams, and how they are related to their fully coherent counterparts; exceptions include the papers of Felde et al. [21], and Soskin and Polyanskii [22]. The vectorial nature of such beams, however, presents more than one way to define singularities related to the state of polarization In this paper, we highlight three ways of characterizing the singularities of a partially coherent electromagnetic wavefield, one of which has previously gone unmentioned. We introduce a simple model of a partially coherent electromagnetic beam possessing a polarization singularity, and examine how that polarization singularity manifests through the different ways of characterizing it.

We begin by reviewing needed definitions related to polarization singularities and coherence, and then discuss the different ways of classifying singularities in partially coherent electromagnetic waves. We then use our model to examine the relationships between the different classifications, and their significance.

1.2 Polarization singularities

In a coherent paraxial electromagnetic wave, the state of polarization is generally elliptical, with the polarization ellipse described by its handedness, angle of orientation Ψ, and ellipticity (ratio of minor to major axis). The most commonly occurring, or generic, singularities in the cross-section of such a beam are C-points and L-lines, which correspond to points of circular polarization and lines of linear polarization, respectively. C-points are singularities in the orientation of the polarization ellipse, and L-lines are singularities in the handedness of the ellipse. We focus on C-points and their non-generic cousins here, which are the most topologically interesting.

C-points may be readily found using the Jones vector of the electric field in a circular polarization basis, which we write as $|\mathbf{E}\rangle_{LR}$. Here "LR" refers to the left-hand circular E_L and right-hand circular E_R complex components of the electric field, with vector dependencies $\hat{\mathbf{x}} + i\hat{\mathbf{y}}$ and $\hat{\mathbf{x}} - i\hat{\mathbf{y}}$, respectively. A point of pure circular polarization will manifest anywhere that one of the complex components vanishes, e.g. $E_L = 0$. The phase θ_L of the component at this point is consequently undefined, making, for example, a right-handed C-point a phase singularity of the scalar component E_L of the field.

C-points are characterized by the behavior of the orientation angle Ψ as one traverses a closed loop around the singular point. This angle must vary continuously with position, except at the C-point itself, and therefore can only change by multiples of 180° around any closed loop. This change is referred to as the topological index n, and may be formally defined by the following integral,

$$n = \frac{1}{2\pi} \oint \mathrm{d}\mathbf{r} \cdot \nabla \Psi(\mathbf{r}). \tag{1.1}$$

The topological index of different polarization singularities is additive: a loop taken around multiple singularities will give an index equal to the sum of the indices of the

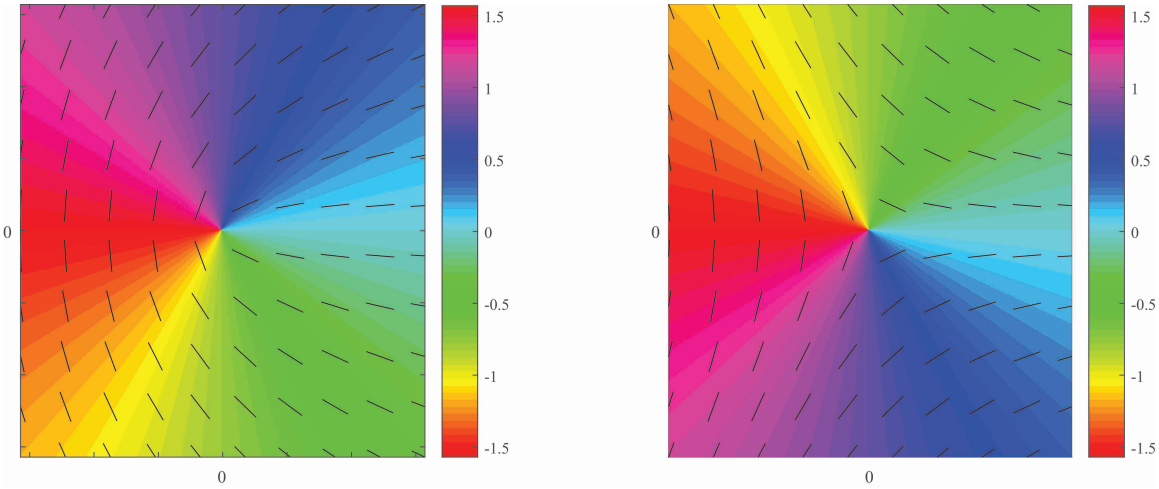

Figure 1.1: Orientation of the major axis of the polarization ellipse for (left) a lemon ($n = 1/2$) and (right) a star ($n = -1/2$), in the plane perpendicular to the optical axis. The major axis is depicted two ways: with lines indicating the major axis direction for selected positions and with a colormap to indicate the value of Ψ.

individual singularities. C-points in particular come in three generic types: lemons with index $n = +1/2$, stars with index $n = -1/2$, and monstars with index $n = +1/2$. The monstar is a less common transition singularity formed in creation and annihilation events between singularities, so we focus on lemons and stars, which are illustrated in Fig. 1.1. In this figure, we illustrate the orientation of the major axis with line segments as well as colors representing the angles.

It is to be noted that the topological index can be readily found from the values of the topological charges of the two components E_L and E_R of the electric field, as we now show. The topological charge t is the net number of 2π changes the phase of the component undergoes in a closed path around the singularity or singularities, and is formally defined as

$$t = \frac{1}{2\pi} \oint \mathrm{d}\mathbf{r} \cdot \nabla\theta(\mathbf{r}), \tag{1.2}$$

where θ is the phase of the particular component.

To determine the relation between the charges of the components and the index of the singularity, we apply some intuition about the properties of the polarization

ellipse. In the LR basis, the two vector components rotate in opposite directions with angles that we label as $\phi_L(\mathbf{r},t)$, $\phi_R(\mathbf{r},t)$. The total field will point along the major axis of the ellipse at a time t_0 when these two angles correspond with the ellipse orientation angle, or

$$\Psi(\mathbf{r}) = \phi_R(\mathbf{r},t_0) = \phi_L(\mathbf{r},t_0). \tag{1.3}$$

But these two rotation angles may be related to the complex phases $\theta_{L,R}(\mathbf{r})$ by the relations

$$\phi_L(\mathbf{r},t) = \omega t - \theta_L(\mathbf{r}), \quad \phi_R(\mathbf{r},t) = \theta_R(\mathbf{r}) - \omega t, \tag{1.4}$$

where ω is the angular frequency of light. We may eliminate the time dependence t_0 from these equations by summing $\phi_L(\mathbf{r},t)$ and $\phi_R(\mathbf{r},t)$; by further using Eq. (1.3), we get the relation

$$\Psi(\mathbf{r}) = \frac{\theta_R(\mathbf{r}) - \theta_L(\mathbf{r})}{2}. \tag{1.5}$$

If we substitute this expression into Eq. (1.1), we readily find that

$$\frac{1}{2\pi}\oint \mathrm{d}\mathbf{r}\cdot\nabla\Psi(\mathbf{r}) = \frac{1}{2}\left\{\frac{1}{2\pi}\oint \mathrm{d}\mathbf{r}\cdot\nabla\theta_R(\mathbf{r}) - \frac{1}{2\pi}\oint \mathrm{d}\mathbf{r}\cdot\nabla\theta_L(\mathbf{r})\right\}. \tag{1.6}$$

Using the definition of topological charge, we have

$$n = \frac{1}{2}(t_R - t_L) = \frac{\Delta t}{2}. \tag{1.7}$$

In short, the topological index can be determined directly from the difference of the enclosed topological charges of the left- and right-handed components; this result was first determined by Angelsky et al. [23].

It is to be noted that this result indicates that polarization singularities of topological index $n = \pm 1/2$ can come in generic and non-generic forms. In the generic form, one component has topological charge unity and the other has topological charge zero,

resulting in a point of circular polarization, and the C-points are the types one expects to see form naturally in random wavefields. However, any case where the topological charges differ by an integer will result in a half-integer topological index, and will have the form of a star or lemon. However, the intensity of the field will be zero at the singularity, and not a point of circular polarization. We refer to these non-generic lemons and stars as *polarization vortices* to distinguish them from C-points.

1.3 Partial coherence in scalar and vector fields

The discussion so far has focused on monochromatic fields. When studying fields that are fluctuating in space and time, one must turn to a statistical description of their behavior. For scalar fields, the preferred quantity of study is the cross-spectral density; for vector fields, the preferred quantity is the cross-spectral density matrix. In this section we briefly review relevant definitions related to these functions.

For a statistically stationary scalar field, the cross-spectral density $W(\mathbf{r}_1, \mathbf{r}_2, \omega)$ of the field at two points $\mathbf{r}_1$ and $\mathbf{r}_2$ may be defined as

$$W(\mathbf{r}_1, \mathbf{r}_2, \omega) = \langle \tilde{U}(\mathbf{r}_1, \omega) U(\mathbf{r}_2, \omega) \rangle_\omega, \tag{1.8}$$

where we use a tilde to represent the complex conjugate and $\langle \cdots \rangle_\omega$ represents an average over an ensemble of monochromatic fields $\{U(\mathbf{r}, \omega)\}$; as first demonstrated by Wolf [24], this ensemble can be created for any partially coherent field. The cross-spectral density is in general frequency dependent, but for quasi-monochromatic fields of central frequency ω_0 the overall behavior of the field can be well-represented by the cross-spectral density evaluated at ω_0; we will consider such cases for simplicity and suppress the frequency dependence in later expressions.

The cross spectral density can be used to directly calculate two important observables of the field: the spectral density $S(\mathbf{r}) = W(\mathbf{r}, \mathbf{r})$ and the spectral degree of coherence $\mu(\mathbf{r}_1, \mathbf{r}_2)$, a normalized quantity that is equal to the visibility of interference

fringes observed when measured with Young's two-pinhole experiment,

$$\mu(\mathbf{r}_1, \mathbf{r}_2) = \frac{W(\mathbf{r}_1, \mathbf{r}_2)}{\sqrt{S(\mathbf{r}_1)S(\mathbf{r}_2)}}. \tag{1.9}$$

As also shown by Wolf [24], the cross-spectral density can always be written in a modal representation called the coherent mode representation, of the form

$$W(\mathbf{r}_1, \mathbf{r}_2) = \sum_s \lambda_s \tilde{\phi}_s(\mathbf{r}_1)\phi_s(\mathbf{r}_2). \tag{1.10}$$

Here, $\lambda_s \geq 0$ is an eigenvalue and $\phi_s(\mathbf{r})$ is an orthonormal eigenfunction of the cross-spectral density, as determined from the relation

$$\int_S W(\mathbf{r}_1, \mathbf{r}_2)\tilde{\phi}_s(\mathbf{r}_1)d^2r_1 = \lambda_s\phi_s(\mathbf{r}_2). \tag{1.11}$$

The domain of integration depends on the geometry of the problem, but is typically taken to be the source plane of a paraxial beam. The summation may be over one or more indices, and may be finite or infinite; for a two-dimensional domain, it is typically a double sum.

The coherent mode representation is a convenient way to illustrate that singularities of phase – associated with zeros of intensity – are not typical features of partially coherent waves. As first noted in Ref. [14], in order for a zero of intensity to appear at a given point, the real and imaginary parts of each mode must simultaneously vanish at that point. If there are N modes, this involves satisfying $2N$ equations with 2 degrees of freedom in a cross-section of the partially coherent beam. This is an overspecified problem unless $N = 1$, which is the fully coherent case. So phase singularities associated with zeros of intensity are not commonly encountered in partially coherent fields.

Phase singularities of two point correlation functions such as the cross-spectral

density, however, are common. The cross-spectral density satisfies a pair of Helmholtz equations, and by fixing one point, say $\mathbf{r}_1 \equiv \mathbf{r}_\mathcal{P}$, the cross-spectral density is equivalent to a monochromatic wave in the other variable, satisfying the Helmholtz equation,

$$[\nabla_2^2 + k^2]W(\mathbf{r}_\mathcal{P}, \mathbf{r}_2) = 0, \tag{1.12}$$

where $k = \omega/c$ and ∇_2^2 is the Laplacian with respect to variable $\mathbf{r}_2$. Just as monochromatic fields will typically possess optical vortices, the cross-spectral density will typically possess *coherence vortices*. It is to be noted, however, that by fixing one point of observation, we are only seeing a projection of the singularity, which exists in a higher-dimensional $\mathbf{r}_1$, $\mathbf{r}_2$ space; studies of the structure of the complete singularity have been done in both the source plane [16] and on propagation [25].

For convenience, we note that the cross-spectral density may be written using bra-ket notation from quantum theory,

$$\begin{aligned} W(\mathbf{r}_1, \mathbf{r}_2, \omega) &= \sum_s \lambda_s \left\langle \mathbf{r}_2 | s \right\rangle_\omega \left\langle s | \mathbf{r}_1 \right\rangle_\omega \\ &= \left\langle \mathbf{r}_2 \right| \boldsymbol{\lambda} \left| \mathbf{r}_1 \right\rangle_\omega , \end{aligned} \tag{1.13}$$

where $\langle r|s\rangle_\omega = \phi_s(\mathbf{r}, \omega)$ and $\boldsymbol{\lambda}$ is equivalent to the usual quantum density operator.

When studying paraxial electromagnetic beams, it is most efficient to decompose them into two orthogonal polarization components $\hat{\mathbf{a}}$ and $\hat{\mathbf{b}}$. Therefore there are four different field correlations to consider, between 4 different scalar modes $E_a(\mathbf{r}_1)$, $E_a(\mathbf{r}_2)$, $E_b(\mathbf{r}_1)$, and $E_b(\mathbf{r}_2)$. In order to deal with this increased complexity, the cross spectral density matrix $\overline{\mathbf{W}}$ is introduced,

$$\begin{aligned} \overline{\mathbf{W}}(\mathbf{r}_1, \mathbf{r}_2) &= \langle \mathbf{E}^\dagger(\mathbf{r}_1) \otimes \mathbf{E}(\mathbf{r}_2) \rangle \\ &= \langle \mathbf{r}_2 | \boldsymbol{\lambda} | \mathbf{r}_1 \rangle . \end{aligned} \tag{1.14}$$

A number of observables of the field may be calculated from this matrix, such as the polarization matrix $\bar{\mathbf{J}}(\mathbf{r}) \equiv \overline{\mathbf{W}}(\mathbf{r},\mathbf{r})$ and the electromagnetic degree of coherence [26], defined as

$$\eta(\mathbf{r}_1,\mathbf{r}_2) = \frac{\mathrm{Tr}(\overline{\mathbf{W}}(\mathbf{r}_1,\mathbf{r}_2))}{\sqrt{\mathrm{Tr}(\bar{\mathbf{J}}(\mathbf{r}_1))\mathrm{Tr}(\bar{\mathbf{J}}(\mathbf{r}_2))}}, \tag{1.15}$$

where Tr represents the trace of the matrix. In analogy with the scalar cross-spectral density, $\overline{\mathbf{W}}(\mathbf{r}_1,\mathbf{r}_2)$ can be written in a coherent mode representation.

$$\overline{\mathbf{W}}(\mathbf{r}_1,\mathbf{r}_2) = \sum_n \lambda_n \mathbf{E}_n^\dagger(\mathbf{r}_1) \otimes \mathbf{E}_n(\mathbf{r}_2) \tag{1.16}$$

or in terms of the density operator

$$\begin{aligned} \overline{\mathbf{W}}(\mathbf{r}_1,\mathbf{r}_2) &= \langle \mathbf{r}_2 | \, \boldsymbol{\lambda} \, | \mathbf{r}_1 \rangle \\ W_{ij}(\mathbf{r}_1,\mathbf{r}_2) &= \langle \mathbf{r}_2, j | \, \boldsymbol{\lambda} \, | \mathbf{r}_1, i \rangle \, , \end{aligned} \tag{1.17}$$

where now $\langle s|\mathbf{r}_1\rangle = \mathbf{E}_s(\mathbf{r}_1)$ represents a vector coherent mode of the field.

1.4 Singularities in partially coherent vector beams

In making a change from scalar beams to vector beams, the singularities of interest change from optical vortices to polarization singularities. In making a change from coherent scalar beams to partially coherent scalar beams, the singularities of interest change from optical vortices to correlation vortices. We now come to the key observation of this article: in going from coherent vector beams to partially coherent vector beams, we end up with more than one way of defining and characterizing the singularities. In this section, we first discuss two known ways of characterizing them and then introduce a third.

The first approach is perhaps the most straightforward: at any given point, i.e. $\mathbf{r}_1 = \mathbf{r}_2 \equiv \mathbf{r}$, we may always uniquely decompose the cross-spectral density into a fully polarized part and a completely unpolarized part, as first illustrated by Stokes

[27] and derived in modern form in Ref. [28]. The polarized part by itself will be a continuous vector field, and will therefore possess C-points that can be characterized as for a fully coherent field, which we refer to as *coherent polarization singularities*. The decomposition may be written in the form

$$\bar{\mathbf{J}}(\mathbf{r}) = \overline{\mathbf{W}}(\mathbf{r},\mathbf{r}) = \bar{\mathbf{J}}_{pol}(\mathbf{r},\mathbf{r}) + \bar{\mathbf{J}}_{unpol}(\mathbf{r},\mathbf{r}). \tag{1.18}$$

The polarized and unpolarized parts may be written as

$$\bar{\mathbf{J}}_{unpol}(\mathbf{r},\mathbf{r}) = \begin{bmatrix} A(\mathbf{r}) & 0 \\ 0 & A(\mathbf{r}) \end{bmatrix}, \tag{1.19}$$

$$\bar{\mathbf{J}}_{pol}(\mathbf{r},\mathbf{r}) = \begin{bmatrix} B(\mathbf{r}) & D(\mathbf{r}) \\ D^*(\mathbf{r}) & C(\mathbf{r}) \end{bmatrix}, \tag{1.20}$$

where

$$A(\mathbf{r}) = \frac{\mathrm{Tr}(\bar{\mathbf{J}}) \pm \sqrt{[\mathrm{Tr}(\bar{\mathbf{J}})]^2 - 4\mathrm{Det}(\bar{\mathbf{J}})}}{2}, \tag{1.21}$$

$$B(\mathbf{r}) = \frac{1}{2}(J_{LL} - J_{RR}) + \frac{1}{2}\sqrt{[\mathrm{Tr}(\bar{\mathbf{J}})]^2 - 4\mathrm{Det}(\bar{\mathbf{J}})}, \tag{1.22}$$

$$C(\mathbf{r}) = \frac{1}{2}(J_{RR} - J_{LL}) + \frac{1}{2}\sqrt{[\mathrm{Tr}(\bar{\mathbf{J}})]^2 - 4\mathrm{Det}(\bar{\mathbf{J}})}, \tag{1.23}$$

$$D(\mathbf{r}) = J_{LR}. \tag{1.24}$$

We may view this characterization of the singularities of the field as looking purely at their vector nature, by focusing on the "diagonal" ($\mathbf{r}_1 = \mathbf{r}_2$) elements of the cross-spectral density. This decomposition was originally formulated in the xy polarization basis, but has the same form in the LR basis.

Working in the LR basis has a particular advantage in studying singularities, however. Because a C-point is defined as a point where the field is circularly polarized, $J_{LR} = 0$ at every C-point. Furthermore, the coherent part of the field can be written

as the direct product of a Jones vector with itself in the LR basis, with components $\mathcal{E}_L(\mathbf{r})$, $\mathcal{E}_R(\mathbf{r})$, such that $J_{LR}(\mathbf{r}) = \mathcal{E}_L^*(\mathbf{r})\mathcal{E}_R(\mathbf{r})$. Since Eq. (1.5) shows that the orientation angle $\Psi(\mathbf{r})$ is directly related to the phases of the LR field components through $2\Psi(\mathbf{r}) = \theta_R(\mathbf{r}) - \theta_L(\mathbf{r})$, the orientation angle of the ellipse for the coherent part of the field can be derived directly from the phase of $J_{LR}(\mathbf{r})$.

It is to be noted that this decomposition cannot be applied globally to the whole beam. As was shown by Wolf [29], it is not in general possible to separate a paraxial vector beam into a polarized beam and unpolarized beam, each of which individually satisfies the wave equation.

An alternative approach for studying the singularities of a vector cross-spectral density is to focus on the analogy with the scalar case, and look for coherence singularities in the directly observable part of the vector field. When performing Young's two-pinhole experiment with partially coherent electromagnetic waves, the visibility of interference fringes is given by $\eta(\mathbf{r}_1, \mathbf{r}_2)$, defined in Eq. (1.15). In analogy with the scalar case, we may find *eta singularities* by fixing one observation point $\mathbf{r}_1 = \mathbf{r}_\mathcal{P}$ and looking for singularities with respect to the second point $\mathbf{r}_2$, i.e. points where $\eta(\mathbf{r}_\mathcal{P}, \mathbf{r}_2) = 0$. As noted by Raghunathan, Schouten and Visser [30, 31], these singularities behave like scalar coherence vortices, with a discrete topological charge. Eta singularities have been relatively unexplored compared to other classes of singularities, though they have been observed in Mie scattering [32] and in the propagation of partially coherent radially polarized beams [33]. Whereas the coherent polarization singularities focused on the diagonal elements of the cross-spectral density matrix in space ($\mathbf{r}_1 = \mathbf{r}_2$), this representation looks at the diagonal elements with respect to polarization, in the form of the trace.

There is a third option, however, that may in a sense be considered a hybrid of the two, or even a generalization. As in the scalar case, we look at the projection of the cross-spectral density on a fixed reference point $\mathbf{r}_\mathcal{P}$. Doing that here leaves us with a

quantity that depends on a single spatial variable $\mathbf{r}_2$, but is still a 2×2 matrix. We now further contract the cross-spectral density matrix with a polarization state $\hat{\mathbf{a}}$ as well.

$$\begin{aligned} \mathbf{W}_{\mathcal{P}\hat{a}}(\mathbf{r}) &= \langle \mathbf{r} | \, \boldsymbol{\lambda} \, | \mathbf{r}_{\mathcal{P}} \rangle \, | \hat{\mathbf{a}} \rangle \\ &= \hat{\mathbf{a}} \cdot \overline{\mathbf{W}}(\mathbf{r}_{\mathcal{P}}, \mathbf{r}). \end{aligned} \tag{1.25}$$

The resultant quantity is a non-uniform complex vector field, which we expect to possess polarization singularities; we refer to these as *partially coherent polarization singularities*. Whereas the two previous classes of singularities essentially simplified the cross-spectral density matrix by diagonalizing in either space or polarization and projecting with respect to the other quantity, here we perform a projection with respect to both space and polarization.

It is to be noted that the cross-spectral density matrix, and consequently the vector $\hat{\mathbf{a}}$, are measured in the LR circular polarization basis. The resulting vector can be written in terms of L and R components as

$$\mathbf{W}_{\mathcal{P}\hat{a}}(\mathbf{r}) = \Big[\; a_R W_{RR}(\mathbf{r}) + a_L W_{LR}(\mathbf{r}), \quad a_R W_{RL}(\mathbf{r}) + a_L W_{LL}(\mathbf{r}) \; \Big]. \tag{1.26}$$

Several questions arise upon seeing the variety of distinct types of singularities that can appear in partially coherent vector beams. The first of these is: how are such singularities related to the singularities of the field in the coherent limit, if at all? The second question is: what is the significance of these different types of singularities? In the next section, we introduce a simple model of a partially coherent vector beam with controllable spatial coherence to answer these questions.

1.5 Construction of model PC beams

To construct a model of a partially coherent beam with a built-in polarization singularity, we will utilize the relationship (1.7) between topological index and topological charge in the LR polarization basis to first construct a coherent field possessing polarization singularities. This field will then be used in a beam wander model to produce the cross-spectral density matrix of a partially coherent non-uniformly polarized beam. The behavior of the beam's singularities can then be analyzed as a function of the spatial coherence.

To model the R and L components of the coherent beam, we will use Laguerre-Gauss beams of radial order 0 and azimuthal order m; we write these modes as $|m\rangle$. We write the particular orders of each component as $m = t_R$ and $m = t_L$.

Written in coordinates natural for vortex beams, $r_\pm = x \pm iy$, and using $t = \alpha m$ where $\alpha = \pm 1$, the field of a scalar component with singularity centered at $\mathbf{c} = (c_+, c_-)$ is, in bra-ket notation,

$$\langle \mathbf{r}|\mathbf{c}, t\rangle = C_m(\sigma^2)(r_\alpha - c_\alpha)^m e^{-|\mathbf{r}-\mathbf{c}|^2/2\sigma^2} e^{ikz}. \tag{1.27}$$

The complex scalar constant $\sigma^2 = w^2(0) + i\frac{z}{k}$; from this we can determine the beam width $w^2(z) = 2|\sigma^2(z)|/\cos(\Phi(z))$ and the Gouy phase, $\Phi = \arg(\sigma^2)$. The fields are taken to be normalized; the normalization factors are included in

$$C_m(\sigma^2) = \frac{1}{\sqrt{m!}} \left(\frac{\cos(\Phi)}{\sigma^2}\right)^{m/2+1}. \tag{1.28}$$

Equation (1.27) describes the behavior of a scalar field at any propagation distance z. An electromagnetic field built from the scalar modes $|\mathbf{c}, t\rangle$ may then be written as

$$|\mathbf{c}, \boldsymbol{\lambda}, \mathbf{t}\rangle = \lambda_L |\mathbf{c}, t_L\rangle |L\rangle + \lambda_R |\mathbf{c}, t_R\rangle |R\rangle. \tag{1.29}$$

To summarize the notation: here t_i represents the topological charge of the ith component, where α_i is its sign and m_i is its magnitude.

Using this model, a coherent beam of $n = 1/2$, for example, could be constructed with $(t_R, t_L) = (m + 1, m)$ for any integer m. The λ_i in the model are complex coefficients whose relative phase affects the orientation of the polarization singularity, and whose magnitudes define how far from the polarization singularity an L-line will manifest. However, the location of singularities in the cross spectral density matrix will be affected by the particular choice made, so they will be taken to both be unity for the remainder of this article.

The beam wander model is a construction of a partially coherent beam through an ensemble of coherent beams with shifted central axes. This model was first used in 2004 [14] to model a partially coherent scalar vortex beam, and may now be considered a special case of a technique for designing genuine correlation functions [34]. The transverse position of the central axis is defined by the central point $\mathbf{c}$ and the probability density of the ensemble is given by $\rho(\mathbf{c})$. For a scalar beam $\Phi(\mathbf{r} - \mathbf{c})$, the cross-spectral density has the form

$$W(\mathbf{r}_{\mathcal{P}}, \mathbf{r}) = \int_{-\infty}^{\infty} \mathrm{d}^2\mathbf{c}\rho(\mathbf{c})\Phi^*(\mathbf{r}_{\mathcal{P}} - \mathbf{c})\Phi(\mathbf{r} - \mathbf{c}). \tag{1.30}$$

The probability density is usually taken to be of Gaussian form, which allows the entire integral to be evaluated analytically.

To create a polarization vortex beam with a prescribed topological index, it is convenient to use separate phase vortex solutions for the R and L components and take advantage of the relationship of their topological charges to index n described in Eq. (1.7). A scalar model of partially coherent Gaussian beams of arbitrary topological charge was introduced by Stahl and Gbur [20], and can be used to apply the beam wander model to the R and L components. To make partially coherent beams carry-

ing lemons and stars, we will expand that model to the electromagnetic case and then choose the azimuthal modes of the L and R components so that $\frac{1}{2}(t_R - t_L) = \pm 1/2$.

The result is the following expression for the cross-spectral density matrix,

$$\overline{\mathbf{W}}(\mathbf{r}_\mathcal{P}, \mathbf{r}) = \int_{-\infty}^{\infty} \mathrm{d}^2\mathbf{c} \;\; \rho(\mathbf{c}) \, \langle \mathbf{r} | \mathbf{c}, 1, \mathbf{t} \rangle \, \langle \mathbf{c}, 1, \mathbf{t} | \mathbf{r}_\mathcal{P} \rangle \,, \tag{1.31}$$

with probability density

$$\rho(\mathbf{c}) = \frac{1}{\pi\delta^2} e^{-c^2/\delta^2}. \tag{1.32}$$

Here δ represents the amount of wander the beam undergoes; $\delta = 0$ represents the coherent limit.

The diagonal terms for this have already been solved in [20], giving

$$W_{ii} = W_g Q_{ii} \sum_{k=0}^{m} \ell! \binom{m_i}{\ell}^2 \left(\tilde{H}_{\alpha_i} H_{\alpha_i} \right)^{m_i - \ell}. \tag{1.33}$$

In this expression, W_g is a Gaussian term dependent on the widths of the mode and the probability density function, Q_{ij} is a coefficient dependent on the topological charges $t_i = \alpha_i m_i$,

$$\begin{aligned} W_g &= \exp\!\left[-\frac{\Delta^2}{4} \left(\frac{2r^2}{\sigma^2\delta^2} + \frac{2r_\mathcal{P}^2}{\tilde{\sigma}^2\delta^2} + \frac{|\mathbf{r} - \mathbf{r}_\mathcal{P}|^2}{|\sigma|^4} \right) \right] \\ Q_{ij} &= \frac{1}{\delta^2} \tilde{C}_i C_j \left(\frac{|\sigma|^2\delta^2}{|\sigma|^2 + \cos\Phi \, \delta^2} \right)^{m_i/2 + m_j/2 + 1} \\ &= \frac{\Delta^2}{\delta^2} \tilde{C}_i C_j \Delta^{m_i + m_j}, \end{aligned} \tag{1.34}$$

and H_i is a complex function that depends on the two coordinates $\mathbf{r}$ and $\mathbf{r}_P$ of the cross-spectral density,

$$H_i(\mathbf{r}_\mathcal{P}, \mathbf{r}) = \Delta \left(\frac{1}{\delta^2} + \frac{1}{2\tilde{\sigma}^2} \right) (x + \alpha_i i y) - \frac{\Delta}{2\tilde{\sigma}^2} (x_\mathcal{P} + \alpha_i i y_\mathcal{P}). \tag{1.35}$$

Furthermore, Δ is a length parameter of the form,

$$\Delta^2 = 2w^2 + w^4/\delta^2. \tag{1.36}$$

It is to be noted that the function W_g possesses no zeros and therefore does not affect the number of singularities or their positions for any of the singularity types considered.

The off-diagonal components of the cross spectral density matrix may be solved in a similar manner, by evaluating the integral,

$$\begin{aligned} W_{ij}(\mathbf{r}', \mathbf{r}) = \frac{\tilde{C}_i C_j}{\pi\delta^2} \int_{-\infty}^{\infty} \mathrm{d}^2 x_c (\tilde{r}'_{\alpha_i} - \tilde{c}_{\alpha_i})^{m_i} (r_{\alpha_j} - c_{\alpha_j})^{m_j} \\ \times e^{-|\mathbf{r}'-\mathbf{c}|^2/2\tilde{\sigma}^2} e^{-|\mathbf{r}-\mathbf{c}|^2/2\sigma^2} e^{-c^2/\delta^2}. \end{aligned} \tag{1.37}$$

Following a procedure analogous to that of Ref. [20], we employ the substitution $\boldsymbol{\rho} = \mathbf{r}_c - \Delta^2(\mathbf{r}_p/\tilde{\sigma}^2 + \mathbf{r}/\sigma^2)/2$, together with binomial expansions of the vortex terms to get the following expression for the off-diagonal elements of $\overline{\overline{\mathbf{W}}}$,

$$\begin{aligned} W_{ij} =& \frac{W_g Q_{ij}}{\pi\Delta^2} \sum_{k=0}^{m_i} \sum_{l=0}^{m_j} \binom{m_i}{k} \binom{m_j}{l} \tilde{H}_i^{m_i-k} H_j^{m_j-l} \\ & \times \int_0^{\infty} \mathrm{d}\rho^2 \Big(\frac{\rho}{\Delta}\Big)^{k+l} e^{-\frac{\rho^2}{\Delta^2}} \int_0^{2\pi} \mathrm{d}\phi \; e^{i(\alpha_j l - \alpha_i k)\phi}. \end{aligned} \tag{1.38}$$

The integral over ϕ is equal to $2\pi\delta_{\alpha_j l - \alpha_i k}$, applying this and a straightforward Gaussian integral compresses our result to the form,

$$\begin{aligned} W_{ij} =& W_g Q_{ij} \sum_{\ell=0}^{m_{min}} \delta_{\alpha_i \ell}^{\alpha_j \ell} \, \ell! \binom{m_i}{\ell} \binom{m_j}{\ell} \tilde{H}_{\alpha_i}^{m_i-\ell} H_{\alpha_j}^{m_j-\ell} \\ =& W_g P_{ij}(r_+, r_-), \end{aligned} \tag{1.39}$$

where P_{ij} is a polynomial factorable into r_+ and r_- terms and m_{min} is the minimum

of $\{m_i, m_j\}$. Using this formula, we can write the cross-spectral vectors, defined in Eq. (1.25), and electromagnetic degree of coherence, defined in Eq. (1.15), in terms of the nonzero W_g and the polynomials P_{ij} in the form

$$\eta = \frac{W_g(P_{RR} + P_{LL})}{\sqrt{\mathrm{Tr}\,[J(\mathbf{r}_\mathcal{P})]\,\mathrm{Tr}\,[J(\mathbf{r})]}}. \tag{1.40}$$

$$\mathbf{W}_{\mathcal{P}\hat{a}} = W_g[\, a_R P_{RR} + a_L P_{LR} \quad a_R P_{RL} + a_L P_{LL}\,] \tag{1.41}$$

Because our expression for the cross-spectral density matrix is analytic, we can directly determine the number of phase singularities each component must possess. Referring to Eq. (1.39) for P_{ij}, we see that the largest powers of the polynomial are of the forms $(x - \alpha_i iy)^{m_i}$ and $(x + \alpha_j iy)^{m_j}$, resulting in m_i and m_j distinct roots, respectively. We may therefore expect that there will be m_i first-order singularities of charge $-\alpha_i$, and m_j first-order singularities of charge $+\alpha_j$.

We may use this observation to determine the singular behavior of the beam for each type of singularity discussed. For coherent polarization singularities, the net topological index, given by Eq. (1.7), will be determined by the zeros of W_{LR}, or

$$n = (-\alpha_L m_L + \alpha_R m_R)/2. \tag{1.42}$$

The topological index of the coherent part of the beam will therefore remain constant, regardless of the state of coherence.

For eta singularities, we combine W_{ii} and W_{jj}. The first term will be a polynomial of order m_i in both $+\alpha_i$ and $-\alpha_i$, and the second term will be a polynomial of order m_j in both $+\alpha_j$ and $-\alpha_j$. Let us consider the case where both $\alpha_i > 0$ and $\alpha_j > 0$, for simplicity. Because the order of a sum of polynomials is the maximum of the orders of the individual polynomials, we find that the number of positive singularities N_η^+

and negative singularities N_η^- is given by

$$N_\eta^+ = N_\eta^- = \max(m_R, m_L). \tag{1.43}$$

The net topological charge will always be zero, though the number of positive and negative charges will depend on the order of the components. For example, a lemon made from $t_R = 3$ and $t_L = 2$ would have 3 pairs of $t = 1$ and $t = -1$ phase vortices.

A similar calculation may be done to determine the number and type of singularities in $\mathbf{W}_{\mathcal{P}\hat{a}}$. We again restrict ourselves to the case where $\alpha_i > 0$ and $\alpha_j > 0$. In this case, the left component of the vector will have $\max(m_R, m_L)$ negative charges and m_L positive charges in general, while the right component of the vector will have m_R positive charges and $\max(m_R, m_L)$ negative charges. The total number of lemons and stars may then be calculated by:

$$N_{lemons} = \text{positive } R\text{+negative } L = m_R + \max(m_R, m_L), \tag{1.44}$$

$$N_{stars} = \text{negative } R\text{+positive } L = m_L + \max(m_R, m_L). \tag{1.45}$$

This assumes that none of the zeros coincide, which is the typical scenario. It is to be noted that the number may change in the special case when the projection vector $\hat{\mathbf{a}}$ is taken to be a pure circular polarization state. By making an appropriate selection of $\hat{\mathbf{a}}$, not only the positions of the polarization singularities but their total number may therefore be manipulated.

1.6 Singularities in model beams

We may now apply our model to investigate and confirm the behavior of the three classes of singularities for partially coherent electromagnetic beams and their relationships to the underlying singularity of the coherent beam. In all examples, we take $w_0 = 0.5$ cm.

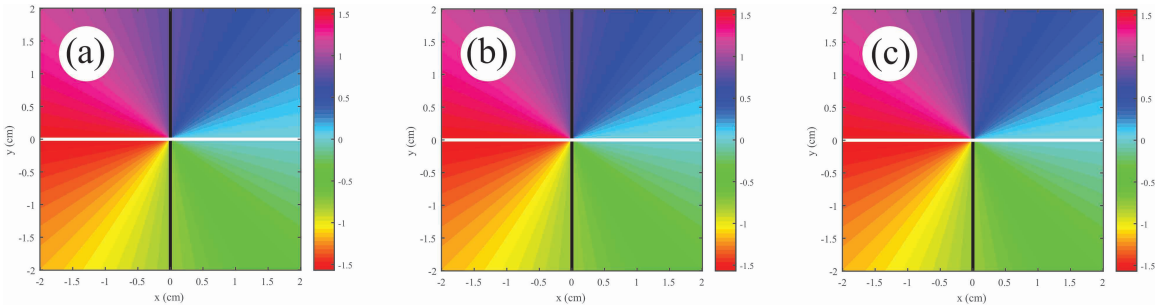

Figure 1.2: Behavior of a coherent polarization singularity as the spatial coherence is decreased, with (a) $\delta = 0.1$ cm, (b) $\delta = 0.5$ cm, (c) $\delta = 3$ cm.

We first consider the case of coherent polarization singularities, characterized by points where $J_{LR}(\mathbf{r}) = 0$, where we take $t_R = 1$, $t_L = 0$, resulting in a generic lemon. Figure 1.2 shows the behavior of the polarization singularity as the spatial coherence is decreased.

It can be seen that the singularity is unchanged in position or even in phase structure as δ is varied. This result is also true for a non-generic lemon, with $t_R = 3$ and $t_L = 2$ (not shown). We may explain this result as arising from the rotational symmetry of all constituent parts of the field: the left and right components of the field, as well as the probability distribution $\rho(\mathbf{c})$, are all symmetric about their central axes. Therefore, there is nothing in the model that provides a direction to break symmetry and allow the position of the polarization singularity to change. This result is noteworthy as it suggests that the coherent polarization singularities maintain their original structure when a beam is randomized under quite general circumstances, and indicates that the topological index will remain unchanged on randomization, as predicted by Eq. (1.42).

The situation for eta singularities, where $\eta(\mathbf{r}_P, \mathbf{r}) = 0$, is significantly different. In Fig. 1.3, there is no eta singularity at the origin in the coherent limit, whereas there is a polarization singularity at that position. This discrepancy arises because eta singularities are associated with a zero of $\mathrm{Tr}[\overline{\mathbf{W}}(\mathbf{r}_1, \mathbf{r}_2)]$, which typically evolves into a zero of intensity in the coherent limit. A generic C-point has a non-zero intensity,

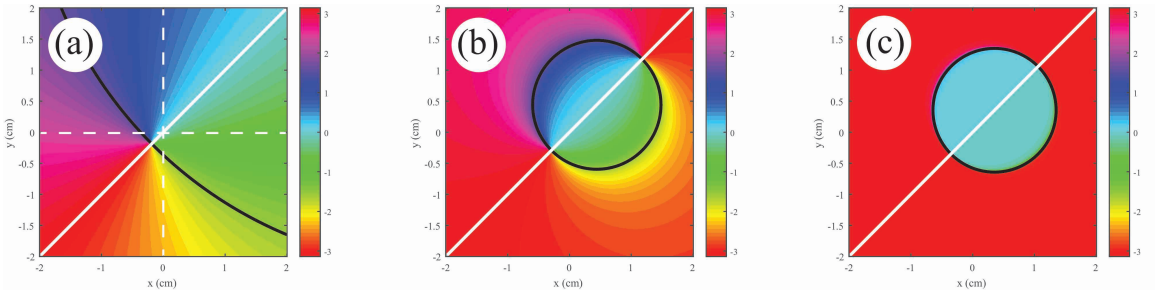

Figure 1.3: Behavior of an eta singularity as the spatial coherence is decreased, with (a) $\delta = 0.1$ cm, (b) $\delta = 0.5$ cm, (c) $\delta = 3$ cm. Here $t_R = 1$, $t_L = 0$ and the observation point is taken at $\mathbf{r}_1 = (0.35, 0.35)$ cm. Dashed lines have been included to show the position of the coordinate system origin.

so this polarization singularity is not directly reflected in the behavior of the eta singularities.

It can be seen that, as the spatial coherence is decreased, a second eta singularity of opposite charge approaches from the point at infinity along the line of $\mathbf{r}_1$, resulting in a field with a net topological charge of zero near the origin. This is the same behavior seen for correlation singularities in scalar fields [14].

For a non-generic polarization vortex, the eta singularity behavior connects more closely to the underlying polarization singularity, as seen in Fig. 1.4. In the coherent limit, the polarization singularity is also a point of zero intensity due to the overlap of zeros of the L and R components of the field. Therefore this corresponds to an eta singularity at the origin, and that eta singularity is preserved as the spatial coherence is decreased.

In Fig. 1.3, we end up with a single plus-minus pair as coherence is decreased, whereas in Fig. 1.4 we end up with three pairs. These results are consistent with the predictions of Eq. (1.43).

We finally consider the behavior of partially coherent polarization singularities where $\mathbf{W}_{\mathcal{P}\hat{a}}(\mathbf{r}) = 0$, where the behavior of such singularities strongly depend on the choice of projection $\hat{\mathbf{a}}$. We may naturally decompose the behavior into the case where $\hat{\mathbf{a}}$ is parallel to the polarized part of the field at the observation point $\mathbf{r}_P$ and the case

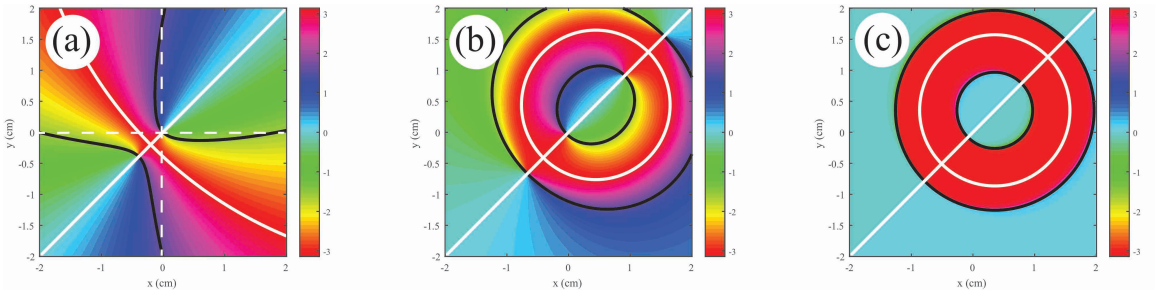

Figure 1.4: Behavior of an eta singularity as the spatial coherence is decreased, with (a) $\delta = 0.1$ cm, (b) $\delta = 0.5$ cm, (c) $\delta = 3$ cm. Here $t_R = 2$, $t_L = 1$ and the observation point is taken at $\mathbf{r}_\mathcal{P} = (0.35, 0.35)$ cm. Dashed lines have been included to show the position of the coordinate system origin.

where $\hat{\mathbf{a}}$ is perpendicular to this polarized part. Figure 1.5 shows the parallel case; we can see that, in the coherent limit, this projection accurately reproduces the lemon behavior at the origin.

The situation is different for the perpendicular case, as shown in Fig. 1.6. The net topological index stays equal to that of the coherent limit, but there are additional singularities present for this case, even as we approach full coherence.

According to Eq. (1.45), we expect to see two lemons and one star in general in the projection as the coherence is decreased, and this is true in both Figs. 1.5 and 1.6. To further confirm that our calculation in Eq. (1.45) is correct, we consider the higher-order polarization vortex case with $t_R = 2$, $t_L = 1$ in Fig. 1.7. Now we predict 4 lemons and 3 stars, which can be seen in Fig. 1.7(c) and (d). It is to be recalled,

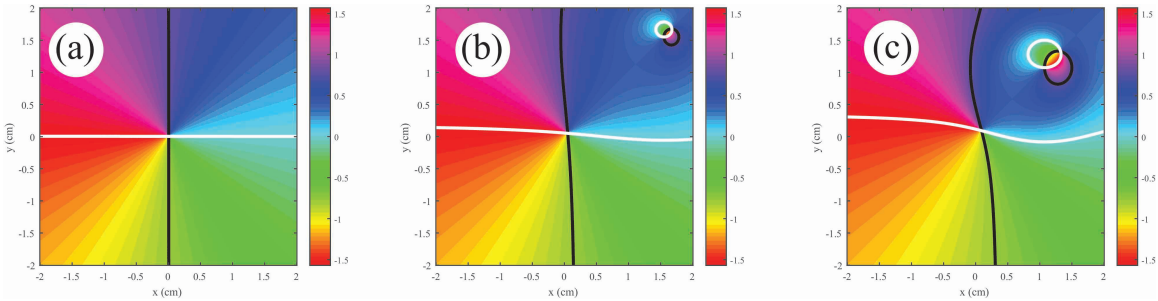

Figure 1.5: Behavior of a partially coherent polarization singularity as the spatial coherence is decreased, with (a) $\delta = 0.1$ cm, (b) $\delta = 0.5$ cm, (c) $\delta = 3$ cm. Here $t_R = 1$, $t_L = 0$ and the observation point is taken at $\mathbf{r}_\mathcal{P} = (0.35, 0.35)$ cm. The unit vector $\hat{\mathbf{a}}$ is taken parallel to the polarized part of the field at $\mathbf{r}_\mathcal{P}$.

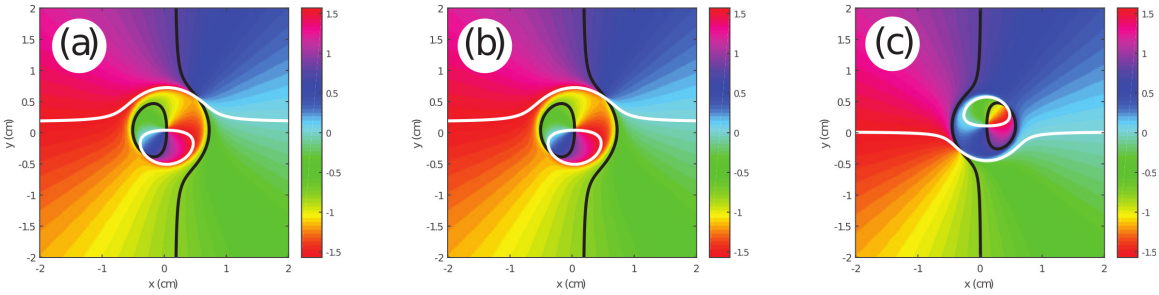

Figure 1.6: Behavior of a partially coherent polarization singularity as the spatial coherence is decreased, with (a) $\delta = 0.1$ cm, (b) $\delta = 0.5$ cm, (c) $\delta = 3$ cm. Here $t_R = 1$, $t_L = 0$ and the observation point is taken at $\mathbf{r}_1 = (0.35, 0.35)$ cm. The unit vector $\hat{\mathbf{a}}$ is taken perpendicular to the polarized part of the field at $\mathbf{r}_{\mathcal{P}}$.

however, that the number of zeros depends on the projection vector $\hat{\mathbf{a}}$; in our case, we find that annihilation events happen in Fig. 1.7(e), resulting in fewer singularities in the low coherence limit.

1.7 Conclusion

Although there is a simple relationship between coherent optical vortices and correlation singularities when looking at scalar wavefields, there are multiple ways to define singularities of a partially coherent vector field. In this article we have discussed three different methods for defining partially coherent vector singularities, and introduced a simple model of a partially coherent vector field to compare them.

Our model demonstrates that, in each case, the singularities that exist in a coherent vector field do evolve into singularities of the cross-spectral density matrix, though each of the partially coherent projections have different relationships to their coherent counterparts. It is to be noted that each of these projections will have their own relevance to experimental observations. The coherent polarization singularities will be reflected in the Stokes parameters of the partially coherent field, whereas the eta singularities and partially coherent polarization singularities will appear in Young's two-pinhole interference experiments, where the fields from two different spatial points are interfered. Furthermore, because the first two methods involve a diagonalized projection of the cross-spectral density matrix in space or polarization,

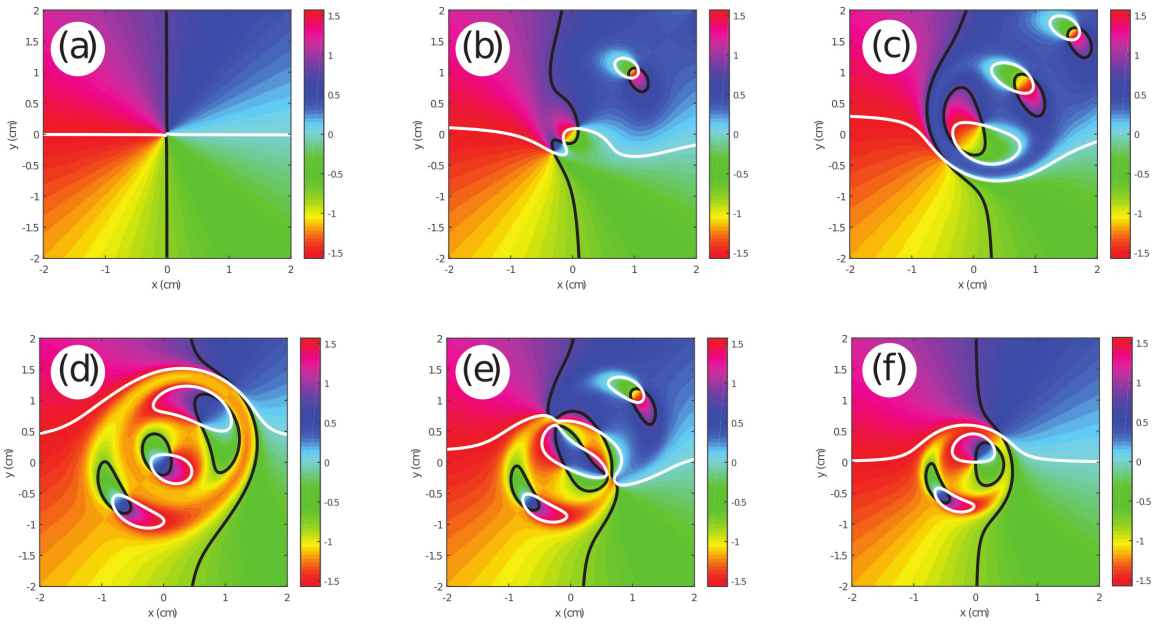

Figure 1.7: Behavior of a partially coherent polarization singularity as the spatial coherence is decreased, with (a),(d) $\delta = 0.1$ cm, (b),(e) $\delta = 0.5$ cm, (c),(f) $\delta = 3$ cm. Here $t_R = 2$, $t_L = 1$ and the observation point is taken at $\mathbf{r}_1 = (0.35, 0.35)$ cm. The unit vector $\hat{\mathbf{a}}$ is taken parallel to the polarized part of the field at $\mathbf{r}_{\mathcal{P}}$ in (a), (b), (c) and perpendicular in (d), (e), (f).

partially coherent polarization singularities cannot be derived from measurements of either of these, and vice-versa. They represent distinct manifestations of singularities in the partially coherent vector case.

It is of interest to note that there is an analogy here to a discussion that arose several years ago, relating to the proper definition of the degree of coherence when dealing with electromagnetic fields. In addition to the aforementioned definition using eta [26], which is determined by the visibility of interference fringes, Tervo et al. [35] simultaneously introduced a definition that stresses the statistical correlations between field components. A third definition was introduced by Réfrégier and Goudail [36] that stresses invariant properties of the field. It appears that the appropriate choice of degree of coherence depends on the interests of the experimenter, and we expect the same is true for the multiple possible definitions of singularities in partially coherent electromagnetic fields.

This article focuses on several definitions of electromagnetic singularities. Like the scalar case [16], however, all these definitions are projections of the true partially coherent electromagnetic singularities which exist in a higher-dimensional space, and which is not easily visualized. Future work will involve trying to determine the nature of such singularities, and it is hoped that the recognition of the various projections will aid in this investigation.

From a practical perspective, we note that there has been much attention paid in recent years to the use of optical vortices in free-space optical communication, which potentially have several advantages over traditional communication schemes [4, 5]. With this in mind, it would seem that beams possessing vector singularities will be a natural next step in research, especially considering that vector beams possess some advantages over scalar beams on propagating in atmospheric turbulence [12]. An understanding of how polarization singularities evolve when the spatial coherence of beams is reduced will be essential for such research, and we hope that this paper is a step in that direction.

Funding

This work was funded by the Air Force Office of Scientific Research (AFOSR) (FA9550-16-1-0240).

CHAPTER 2: EVOLUTION OF THE POLARIZATION SINGULARITIES IN PARTIALLY COHERENT BEAMS ON PROPAGATION THROUGH TURBULENCE

abstract

In recent years, topological singularities of wavefields have been considered as structures that can improve a variety of optical technologies, including remote sensing and free-space optical communications. However, atmospheric turbulence can distort the features of singularities over long propagation distances, limiting their use in many cases. One solution being considered is the reduction of spatial coherence of light, as partially coherent beams have shown increased resistance to turbulence under a broad range of situations. In this paper, we look at the evolution of polarization singularities that arise in a particular projection of a partially coherent vector beam, and how the position and number of singularities are affected by atmospheric turbulence. We find that there are projections where the singularities persist on propagation, suggesting their possible use in applications.

2.1 Introduction

In recent years, significant effort has focused on the science and applications of wavefield singularities, becoming a subfield of optics in its own right known as singular optics [3, 2, 37]. The most familiar form of such singularities are optical vortices in scalar fields, which are lines of zero intensity in three-dimensional space around which the field has a circulating or helical phase [38, 39]. These vortices are topological structures of the wavefield, and for monochromatic waves the phase always increases or decreases by an integer multiple of 2π; this multiple is called the topological charge,

t, of the vortex.

Entire classes of beams can be constructed with optical vortices on their central axis; the most notable of these are the Laguerre-Gauss beams, where the azimuthal order l of the Laguerre-Gauss mode represents the topological charge of the beam [40]. Because vortices are discrete features of a wavefield that are robust under small perturbations, vortex beams have been considered as a means to increase the stability and data transmission rate in free-space optical communications. One way this can be done is by using different Laguerre-Gauss modes, which can be multiplexed and demultiplexed optically, as independent data channels [41, 5]; the individual modes will be distorted by atmospheric turbulence, however, resulting in modal crosstalk [42]. An alternative is to use different vortex orders as an "alphabet" to replace binary data information; it has been shown that vortices can travel long distances in turbulence without distortion [43]; however, one must measure the phase of the wavefield at the detector to extract the vortex information.

Vortices are the natural singularities in beams with a uniform state of polarization. However vector beams, which have a nonuniform state of polarization in their cross-section, instead possess singularities in the structure of the polarization ellipse, and the typical type of singularities in this case are points where the polarization is circular and the ellipse orientation is undefined [44]. A discrete topological index can be associated with polarization singularities that takes on half-integer values, and these singularities are also robust under perturbations of the field. These properties suggest that polarization singularities could also be used as an alternative carrier of data in free-space optical communications, with additional robustness due to the nonuniform polarization; it has been shown that certain classes of nonuniformly polarized beams have reduced intensity fluctuations in turbulence [12].

Another way to reduce the intensity fluctuations of beams in turbulence is to make the beams partially coherent [45]. A beam with reduced spatial coherence is in a sense

"pre-randomized" and will have fewer self-interference effects, reducing scintillations. Optical vortices do not typically appear in such beams, but vortices can appear in the two-point correlation function of a partially coherent beam, and these vortices are also robust [46].

When a vector field is also partially coherent, even richer possibilities for wavefield singularities appear. Recently, we demonstrated that one can envision three different and largely independent types of singularities in vector partially coherent fields [47]. The first of these are polarization singularities in the fully polarized part of the field; the second are scalar singularities in the degree of coherence of the field. The third type are projections of the correlation matrix of the field onto a single polarization state and observation point, which results in a set of polarization singularities in the resulting vector field. This third class of singularities, like its partially coherent scalar and coherent vector counterparts, might prove useful in transmitting data through free-space.

In this paper, we look theoretically at atmospheric propagation of a class of partially coherent vector beams carrying singularities. We look at the evolution of the projected polarization singularities on propagation and their dependence on the source and turbulence parameters.

2.2 Characterizing partially coherent vector beams and their singularities

A partially coherent field is randomly fluctuating in space and time, usually at a rate too fast for a detector to measure. Optical coherence theory is therefore typically concerned with averages of field quantities over an ensemble of realizations that, assuming ergodicity, is equivalent to a long time average. For scalar fields, the observable properties of the field are characterized by a two-point correlation function, the cross-spectral density, that is defined as

$$W(\boldsymbol{p}, \boldsymbol{q}, \omega) = \langle U^*(\boldsymbol{p}, \omega) U(\boldsymbol{q}, \omega) \rangle_\omega \,, \tag{2.1}$$

where $\boldsymbol{p}$ and $\boldsymbol{q}$ represent the position vectors of two points within the field and the brackets $\langle\rangle_\omega$ represent an average over an ensemble of a monochromatic field realizations $U(\boldsymbol{p},\omega)$, as first introduced by Wolf [48]. In most applications, fields are quasi-monochromatic and can be well-described by their central frequency ω; we assume this to be the case moving forward and suppress expression of ω.

We are most interested in highly directional beam-like fields, for which the polarization vector lies in a plane perpendicular to the direction of propagation. If the state of polarization is nonuniform and varies within the beam's cross-section, possibly in a random manner, the beam must be characterized by a cross-spectral density matrix defined as [49]

$$\begin{aligned}\overline{\mathbf{W}}(\boldsymbol{p},\boldsymbol{q}) &= \langle \boldsymbol{E}^\dagger(\boldsymbol{p}) \otimes \boldsymbol{E}(\boldsymbol{q})\rangle \\ &= \begin{pmatrix} \langle E_1^*(\boldsymbol{p})E_1(\boldsymbol{q})\rangle & \langle E_1^*(\boldsymbol{p})E_2(\boldsymbol{q})\rangle \\ \langle E_2^*(\boldsymbol{p})E_1(\boldsymbol{q})\rangle & \langle E_2^*(\boldsymbol{p})E_2(\boldsymbol{q})\rangle \end{pmatrix},\end{aligned} \tag{2.2}$$

where $\boldsymbol{E}(\boldsymbol{p})$ represents the transverse electric field at point $\boldsymbol{p}$, $E_i(\boldsymbol{p})$ represents the ith transverse component, with $i = 1, 2$ and $\otimes$ represents the outer product of vectors.

The cross spectral density matrix includes the case $\boldsymbol{p} = \boldsymbol{q} = \boldsymbol{r}$, which provides the relative correlations between field components at a single point; these correlations characterize the state of polarization. More details of the properties of the cross-spectral density matrix can be found in Wolf [28].

In a partially coherent scalar beam, the singularities are pairs of points in the beam cross-section where the cross-spectral density vanishes and the phase of the cross-spectral density is therefore undefined. In a coherent vector beam, the singularities are points where the orientation of the polarization ellipse, characterized by the azimuthal angle Ψ of the major axis of the ellipse, is undefined. This is typically in the form of an isolated point of circular polarization or a "C-point," but also includes higher-order singularities where the field intensity is zero, often called "V-points" [50].

For the cross spectral density matrix of partially coherent vector beams, there are in fact multiple types of vector field singularities that can be characterized. In our earlier work [47], we outlined three ways to define singularities in $\overline{\mathbf{W}}(\boldsymbol{p}, \boldsymbol{q})$. The most straightforward of these methods is to look at the singularities of the polarized part of the field, derived from $\overline{\mathbf{W}}(\boldsymbol{r}, \boldsymbol{r})$. This case manifests singularities that are essentially the same as those of a fully coherent polarized beam, and therefore this case provides little novelty. The second method is to look at scalar singularities of the electromagnetic degree of coherence $\eta(\boldsymbol{p}, \boldsymbol{q})$, defined as

$$\eta(\boldsymbol{p}, \boldsymbol{q}) \equiv \frac{\mathrm{Tr}[\boldsymbol{W}(\boldsymbol{p}, \boldsymbol{q})]}{\sqrt{\mathrm{Tr}[\boldsymbol{W}(\boldsymbol{p}, \boldsymbol{p})]\mathrm{Tr}[\boldsymbol{W}(\boldsymbol{q}, \boldsymbol{q})]}}, \tag{2.3}$$

where Tr indicates the trace of the matrix. This method results in singularities that do not appear to be directly connected with the polarization singularities of the field.

The most promising method of defining singularities in $\overline{\mathbf{W}}(\boldsymbol{p}, \boldsymbol{q})$ is to project the matrix onto a fixed point $\boldsymbol{p}$ and polarization state $\boldsymbol{a}$, where $\boldsymbol{a}$ is a generally complex unit vector. This projection can be written formally as

$$\boldsymbol{W}_{\boldsymbol{a},\boldsymbol{p}}(\boldsymbol{q}) \equiv \boldsymbol{a} \cdot \boldsymbol{W}(\boldsymbol{p}, \boldsymbol{q}), \text{ with } \boldsymbol{p} \text{ fixed.} \tag{2.4}$$

This projection itself behaves as an ordinary vector beam, and we may define a polarization ellipse for this beam with orientation $\Psi(\boldsymbol{q})$; this vector beam can therefore possess its own polarization singularities. Formally, we should refer to these as polarization singularities of a projection of a vector partially coherent beam, but going forward we will simply refer to them as polarization singularities. These projected polarization singularities are the only ones we will concern ourselves with in this paper.

The projected vector field can be thought of as a cross-section of the singularities of the full cross-spectral density matrix in the higher dimensional space that defines

$\boldsymbol{W}(\boldsymbol{p}, \boldsymbol{q})$. This space is defined by allowing both $\boldsymbol{p}$ and $\boldsymbol{q}$ to vary in the cross-section of the beam, and is effectively a four-dimensional space. The singularities that appear at isolated points $\boldsymbol{q}$ for fixed values of $\boldsymbol{p}$ will become surfaces when $\boldsymbol{p}$ is allowed to vary as well, suggesting the singularities form two-dimensional surfaces in our four-dimensional space. Similar singular surfaces have been investigated for scalar wavefields [51] and are well-defined but hard to visualize. The difficulties associated with this are only exasperated by allowing the coordinates of the projected $\boldsymbol{a}$ on the Poincaré sphere to vary as well, adding two more dimensions to the space and the manifold describing the singularities. The projection of Eq. (2.4), in contrast, has well-defined polarization singularities with half-integer values of topological index, and these singularities are expected to be somewhat robust under perturbations such as turbulence.

If we consider the complete propagated field instead of its behavior in a transverse plane, the cross-spectral density matrix $\boldsymbol{W}(\boldsymbol{p}, \boldsymbol{q})$ becomes an effectively six-dimensional space, as $\boldsymbol{p}$ and $\boldsymbol{q}$ are now three-dimensional spatial vectors. However, we almost always study the cross-spectral density matrix in a single transverse cross-section, so we are only considering an effectively five-dimensional space. In this case, with $\boldsymbol{p}$ fixed, our singular points become singular lines.

Even if we construct a cross-spectral density matrix from an ensemble of vector beams with a pure polarization singularity on the optical axis, we anticipate additional singularities may be present in our projections due to the effects of partial coherence. On propagation in free space, the field will become increasingly coherent in accordance with the van Cittert-Zernike theorem (see, for example, [28]). It is expected that the additional singularities will therefore disappear or have some measure of viability approach zero as the propagation distance increases. For a beam propagating in the atmosphere, however, turbulence is a source of coherence loss for the beam, and part of our objective will be to see how these competing processes of increasing and

decreasing coherence affect the singularities of the beam.

2.3 Model of partially polarized vector vortex beam

We are interested in a model of a partially polarized vector vortex beam that in its coherent limit corresponds to a vector vortex beam with a specified topological index. The most common model used is of Gaussian Schell-model type, one form of which can be written as

$$\boldsymbol{W}(\boldsymbol{p},\boldsymbol{q}) \equiv \boldsymbol{E}^{\dagger}(\boldsymbol{p}) \otimes \boldsymbol{E}(\boldsymbol{q}) \exp[-R^2/\sigma_{\mu}^2], \tag{2.5}$$

where $\boldsymbol{E}(\boldsymbol{p})$ is a coherent vector vortex beam and the Gaussian function represents the spatial degree of coherence between different points in space, with $\boldsymbol{R} = \boldsymbol{q} - \boldsymbol{p}$, and σ_{μ} is the correlation length of the beam. Gaussian Schell-model beams are well-known to lose their singularities on propagation, even in free space, making them less than ideal for atmospheric applications. They also a topology for the projection of $\overline{\mathbf{W}}$ in the defined cross section which is indistinguishable from the polarization singularities of the coherent beam $\boldsymbol{E}$ used to define it and so includes none of the novelty of partially coherent polarized beams we are studying.

We instead use a so-called beam wander model for a partially coherent singular beam, in which the cross-spectral density is constructed out of an ensemble of identical coherent vector vortex beams with shifted center axes. In the scalar case, entire classes of beam wander model beams have been constructed out of every azimuthal order Laguerre-Gauss beam [52] and every radial order Laguerre-Gauss beam [53], and in the latter case it was shown that the singularities of such beams become more prominent and deterministic as they propagate in free space.

We may construct a vector vortex beam of arbitrary topological index from scalar vortex beams with orthogonal circular polarization states. If we construct a beam from a left circularly polarized beam of topological charge t_L and a right circularly

polarized beam of topological charge t_R, it has been shown [23] that the topological index n of the resulting polarization singularity has the value

$$n = \tfrac{1}{2}(t_R - t_L). \tag{2.6}$$

It is to be noted that this expression implies that we can make different choices of t_R and t_L that will result in the same n and will result in the same overall topological structure of Ψ. C-points arise when either $t_R = 0$ or $t_L = 0$; if both are non-zero we get a V-point.

For our scalar vortex beams $\Phi_i(\boldsymbol{r})$, with $i = L, R$, we take the familiar Laguerre-Gauss beams of radial order zero and azimuthal order $t_i = \pm_i m_i$, where $m_i = |t_i|$. Here the symbol $\pm_i$ represents the sign of the ith component, which may be taken to be positive or negative; $\mp_i$ is $\pm_i$ multiplied by -1. These may be written in compact form as

$$\Phi_i(\boldsymbol{r}) = A_i \frac{\sigma_o^2}{\sigma^2\sqrt{m_i!}} \left(\frac{\sigma_o r_{\pm_i}}{\sigma^2}\right)^{m_i} \exp\left[-\tfrac{r^2}{2\sigma^2}\right], \tag{2.7}$$

where A_i is the overall amplitude and $r_\pm = x \pm iy$. We have introduced a complex parameter σ^2 with dimension of area and constant real part σ_o^2; this accounts for the Gaussian beam properties such as beam width w, wavefront curvature F and the Gouy phase Φ_G. Because we will construct our partially coherent beams out of shifted copies of these scalar beams, the overall topological index of the polarized part of the beam will remain unchanged regardless of the state of coherence.

In the beam wander model, the cross spectral density matrix may be constructed from a weighted incoherent sum of identical vector beams with shifted centers $\boldsymbol{c}$, of the form

$$\overline{\mathbf{W}}(\boldsymbol{p}, \boldsymbol{q}) = \int \mathrm{d}^2 c\, \lambda(\boldsymbol{c}) \boldsymbol{\Phi}^\dagger(\boldsymbol{p} - \boldsymbol{c}) \otimes \boldsymbol{\Phi}(\boldsymbol{q} - \boldsymbol{c}), \tag{2.8}$$

where

$$\lambda(\boldsymbol{c}) = (\pi\sigma_\lambda^2)^{-1}\exp[-c^2/\sigma_\lambda^2] \tag{2.9}$$

is the probability density of the ensemble of transverse $\boldsymbol{c}$-values, σ_λ is the variance of the distribution, and $\boldsymbol{\Phi}(\boldsymbol{q}-\boldsymbol{c})$ is one of the vector beams constructed from the scalar components of Eq. (2.7). This construction was originally called the "beam wander model" because the random axial position of the ensemble members is a rough approximation of the beam wander experienced by coherent beams propagating through atmospheric turbulence; the beams are now also called Rankine vortex beams because of the Rankine vortex nature of their orbital angular momentum [54, 55]. As the wander of the beam is increased, the spatial coherence of the beam decreases.

For notational simplicity, we introduce a parameter γ_α as an inverse squared width, with $\gamma_\alpha = \sigma_\alpha^{-2}$, where the subscript α can refer to a number of different defined widths. In this notation, σ_α always has dimension of length and γ_α, if complex, may be written $\gamma_\alpha = \gamma'_\alpha + i\gamma''_\alpha$. Hence the Laguerre-Gauss mode of Eq. (2.7) can be written compactly as

$$\Phi_i(\boldsymbol{r}) = C_i\gamma^{m_i+1}r_{\pm_i}^{m_i}\exp(-\gamma r^2/2), \tag{2.10}$$

where C_i is a constant of units $\mathrm{m}^{m_i}\mathrm{N/C}$ and γ is in reference to the beam width σ. We also take $\gamma_\lambda = \sigma_\lambda^{-2}$.

We may now evaluate the integral of Eq. (2.8), which can be done analytically because of the choice of a Gaussian for the probability density of Eq. (2.9) and Laguerre-Gauss modes for the members of the ensemble. The method follows the same approach of our previous paper [47], and we may write the i,jth component of

the cross-spectral density matrix as

$$W_{ij}(\boldsymbol{p},\boldsymbol{q}) = A_W W_{ij}^{(s)}(\boldsymbol{p},\boldsymbol{q}) e^{-\frac{1}{2}\gamma_1^* p^2 - \frac{1}{2}\gamma_1 q^2 - \frac{1}{4}\gamma_2 R^2}, \tag{2.11}$$

$$W_{ij}^{(s)}(\boldsymbol{p},\boldsymbol{q}) = \; C_i^* C_j \sum_{\ell=0}^{m} c_{ij\ell} \gamma_s^\ell P_i^{m_i-\ell} Q_j^{m_j-\ell}, \tag{2.12}$$

$$Q_i(\boldsymbol{p},\boldsymbol{q}) = \gamma_1 q_{\pm_i} + \tfrac{1}{2}\gamma_2 R_{\pm_i}, \tag{2.13}$$

$$P_i(\boldsymbol{p},\boldsymbol{q}) = Q_i^\dagger = \gamma_1^* p_{\mp_i} - \tfrac{1}{2}\gamma_2 R_{\mp_i}, \tag{2.14}$$

where again $\boldsymbol{R} = \boldsymbol{q} - \boldsymbol{p}$, $\dagger$ represents the Hermitian conjugate with respect to the coordinates $\boldsymbol{p}$ and $\boldsymbol{q}$, and the coefficient $c_{ij\ell} = \ell!\binom{m_i}{\ell}\binom{m_j}{\ell}$. In the summation, the the upper limit m is lowest common degree of polynomial between i and j and so is the minimum of m_i and m_j when the two charges have the same sign and is 0 when they do not; The γ_α parameters for our model have the forms,

$$\gamma_1 = \gamma \frac{\gamma_\lambda}{\gamma_\lambda + \gamma'}, \tag{2.15}$$

$$\gamma_s = \frac{|\gamma|^2}{\gamma_\lambda + \gamma'}, \tag{2.16}$$

$$\gamma_2 = \gamma_s \; . \tag{2.17}$$

In the coherent limit, i.e. $\gamma_\lambda \to \infty$, $\gamma_1 \to \gamma$ and $\gamma_s \to 0$, only the $l = 0$ term of the sum survives and the cross-spectral density matrix factorizes into the product of two coherent Laguerre-Gauss modes of the form of Eq. (2.7).

If we consider $\boldsymbol{J}(\boldsymbol{r}) \equiv \overline{\mathbf{W}}(\boldsymbol{r},\boldsymbol{r})$, only γ_1 and γ_s appear with γ_1 giving the waist and Gouy phase while γ_s indicates coupling of the original beam modes into lower-order modes through a reduction of spatial coherence.

We have separated out the term $W_{ij}^{(s)}(\boldsymbol{p},\boldsymbol{q})$ in the cross-spectral density matrix because the complex exponentials are the same across all components and possess no zeros, which means that they do not add any topological features to the beam. The

topology of $\overline{\overline{\mathbf{W}}}$ can therefore be analyzed by studying the topology of $\overline{\overline{\mathbf{W}}}^{(s)}$ alone. If we now consider the projection of the matrix defined by Eq. (2.4), we may write

$$\begin{aligned}\overline{\overline{\mathbf{W}}}_{\boldsymbol{a}}^{(s)} &= \left[a_R \overline{\overline{\mathbf{W}}}_{RR}^{(s)} + a_L \overline{\overline{\mathbf{W}}}_{LR}^{(s)} \qquad a_R \overline{\overline{\mathbf{W}}}_{RL}^{(s)} + a_L \overline{\overline{\mathbf{W}}}_{LL}^{(s)} \right] \\ = |a_R^2 C_R^2| \sum_{\ell=0}^{M} \ell! \, \gamma_2^{\ell} \left[(\rfloor \binom{M}{\ell} P_{\mp}^{M-\ell} + \beta_{\boldsymbol{a}} \beta_C^* \binom{m}{\ell} P_{\mp}^{m-\ell} \right] & \left[\binom{M}{\ell} Q_{\pm}^{M-\ell} \quad \beta_C \binom{m}{\ell} Q_{\pm}^{m-\ell} \right] ,\end{aligned} \tag{2.18}$$

where the topology is only dependent on the complex ratios $\beta_{\boldsymbol{a}} = a_L/a_R$ and $\beta_C = C_L/C_R$. This projection will have singular points in Ψ where either ${W_{\boldsymbol{a}}^{(s)}}_R$ or ${W_{\boldsymbol{a}}^{(s)}}_L$ are zero.

The number of zeros for a polynomial of one complex variable is the degree of the polynomial; for most cases under consideration the number of zeros is equal to the sum of zeros of q_+ and q_-. In the case of $\pm_i 1 = \pm_j 1 = \pm 1$, the right circular component is a polynomial of m_R degrees in $q_\pm$ and $m_{\max} = \max(m_R, m_L)$ degrees in $q_\mp$. For the case of $t_i = m_i$ this implies that the right circular component will introduce up to m_R C-points with topological index of $n = 1/2$ ("lemons") and $\max(m_R, m_L)$ C-points with topological index of $n = -1/2$ ("stars"), with left circular polarization at the singularities. The zeros of the left circular component indicate there will be up to m_L stars and $\max(m_R, m_L \delta_{\pm_i 1}^{\pm_j 1})$ lemons with right circular polarization. The index of the total beam is therefore

$$n = \pm \left[\tfrac{1}{2}(m_R + m_{\max}) - \tfrac{1}{2}(m_L + m_{\max}) \right] = \tfrac{1}{2}(t_R - t_L), \tag{2.19}$$

which is the desired topological index of the beam.

However, there are

$$N_s = m_R + m_L + 2\max(m_R, m_L) \tag{2.20}$$

total singular points in this case rather than one singular point at the optical axis

as is the case for a coherent and Gaussian Schell beam. Putting in reasonable values for the parameters γ_o, γ_λ and $\boldsymbol{C}$ showed that our analysis correctly determines the number and types of singularities that exist for the cases $\boldsymbol{t} = (1 \;\; 0)$ and $\boldsymbol{t} = (2 \;\; 1)$, where $\boldsymbol{t} = (t_R \;\; t_L)$, in the cross-section of the beam in the source plane.

However, there are cases where the number of singularities is not equal to the polynomial degrees in this way. For example, when γ_1 is complex, the number of singularities can be reduced by multiples of two. Because a complex γ_1 is equivalent to free space propagation of the beam, we will address these cases in Section 2.5.

Let us analyze the case of $\boldsymbol{t} = (1 \;\; 0)$, chosen because of its simplicity and because its singularity is a familiar C-point. Our example, when projected onto the state $\boldsymbol{a}$, gives

$$\overline{\overline{\mathbf{W}}}^{(s)}_{\boldsymbol{a}} = a_R |C_R^2| \left(\left(P_{\mp} + \beta_{\boldsymbol{a}} \beta_C^* \right) \begin{bmatrix} Q_{\pm} & \beta_C \end{bmatrix} + \begin{bmatrix} \gamma_s & 0 \end{bmatrix} \right), \tag{2.21}$$

and the zeros of its vector components correspond to the partially coherent polarization singularities. Let us consider how the position of the singularities depends on the choice of projection, in particular the major axis angle of the projection and the ratio $\beta_{\boldsymbol{a}}$.

The zero in the left circular component is located at

$$q_{\pm} = p_{\pm} + \frac{\gamma_1}{\gamma_2} p_{\pm} + \frac{2}{\gamma_2} |\beta_C \beta_{\boldsymbol{a}}| e^{2\Psi_{\boldsymbol{a}} - 2\Psi_0} \tag{2.22}$$

where the major axis of the coherent mode used in the beam wander model is $\Psi_\Phi = \phi/2 + \Psi_0$. If we consider a constant $|\beta_{\boldsymbol{a}}|$ and vary Ψ_Φ, we see that this singularity is located on a circle and all positions on the circle are covered as the major axis goes through all possible orientations.

The two zeros of the right circular component do not have clean analytical solutions but setting $\overline{\overline{\mathbf{W}}}^{(s)}_{\boldsymbol{a}\;R} = 0$ defines the real and imaginary parts as circles, the intersection of which are the singularities. The positions of the three singularities present, as a

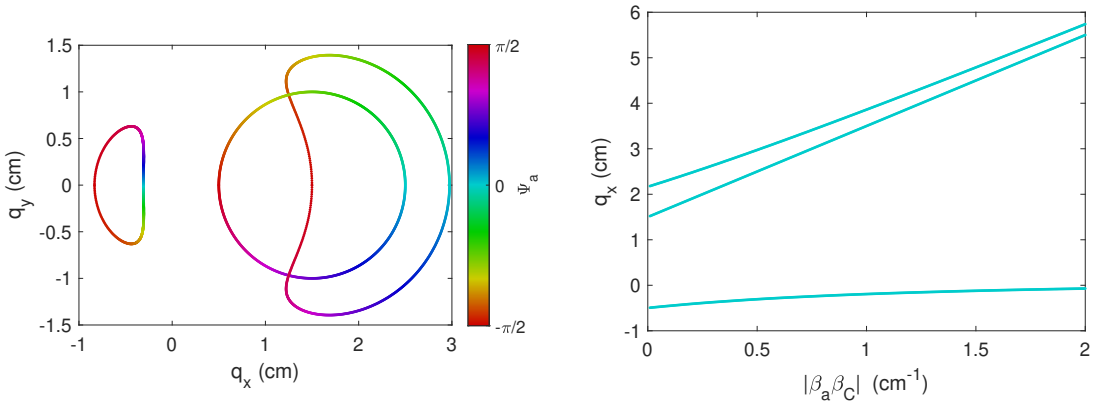

Figure 2.1: The position of the polarization singularities as the projection vector $\boldsymbol{a}$ is changed. In (a), the singularity is projected onto a state where only the orientation, $\Psi_{\boldsymbol{a}}$, of the polarization used in the projection is varied while the eccentricity is set so that $|\beta_{\boldsymbol{a}}\beta_C| = 0.5\,\mathrm{cm}^{-1}$. The color of each point along the line of singularity indicates the angle $\Psi_{\boldsymbol{a}}$ for which the singularity is located at the point shown. In (b), the singularity is projected onto a state with a constant major axis $\Psi_{\boldsymbol{a}} = 0$ with $|\beta_{\boldsymbol{a}}\beta_C|$ varied. All γ_i are measured in cm^{-2} and we project onto $\boldsymbol{p} = (0.5\ \ 0)$ cm.

function of the major axis angle, are shown in Fig. 2.1(a).

In general, a change in $\Psi_{\boldsymbol{a}}$ causes rotation of the position of the singular points near the axis while increases in $|\beta_{\boldsymbol{a}}\beta_C|$ move those points away from the beam center. The one exception for this example beam occurs when for $\beta_{\boldsymbol{a}}\beta_C^*$ is real and negative, meaning $\Psi_{\boldsymbol{a}}$ is perpendicular to the polarized part of the beam at $\boldsymbol{p} = p_x\hat{x}$, when the magnitude is such that $\overline{\mathbf{W}}_{\boldsymbol{a}}^{(s)}$ is real everywhere. In that projection a degenerate singularity in the form of a circle replaces a pair of singular points. Similarly, for higher order beams there will be regions in the space of $\boldsymbol{a}$ is where the projection will possess extra pairs of singularities. However, for these models the number of singular lines in the space $(q_x, q_y, |\boldsymbol{a}|)$ stays the same.

In free-space propagation, the topological index of the beam will be generally conserved, but the number of singularities is not a constant of the beam: singular points may overlap and become a single point of different index or they may annihilate each other completely if they have equal and opposite indices. They also will change location as z increases, possibly moving towards or away from the optical axis, increasing

or decreasing their visibility at the detector. What changes occur, and when, can only be answered if we extend our model of $\overline{\mathbf{W}}$ to $\overline{\mathbf{W}}(\boldsymbol{p}, \boldsymbol{q}, z)$. We incorporate a discussion of free space propagation in our discussion of turbulence propagation, as free space is the limiting case of extremely weak turbulence.

2.4 Propagation of the model

Atmospheric turbulence is modeled as random variations of the index of refraction $n(\boldsymbol{r}, t)$ in space and time, treated statistically with an ensemble of turbulence realizations that are effectively static on the time scale of beam propagation. The variations of refractive index induce random phase fluctuations on any beam propagating through them, and the general result is a loss of beam coherence. The statistical properties of the atmosphere are modeled by a spatial frequency power spectrum; in this paper we use a Gaussian power spectrum for the sake of analytic tractability. Such a power spectrum is a fair approximation for many turbulent conditions, and we are more concerned with the effects of a random medium on the beam topology than how a specific turbulence model affects the propagation.

In free space, the paraxial propagation of a beam can be modeled using Rayleigh-Sommerfeld diffraction, in the form

$$\boldsymbol{E}(\boldsymbol{r}, z) = \frac{\varphi_d}{2\pi} e^{ikz} \int\int \mathrm{d}^2 r' \boldsymbol{E}(\boldsymbol{r}', 0) \exp\left(-\tfrac{1}{2}\varphi_d |\boldsymbol{r} - \boldsymbol{r}'|^2\right), \tag{2.23}$$

where $\varphi_d \equiv -ik/z$. We may use Eq. (2.2) to write the components of the cross-spectral density matrix as

$$\begin{aligned} W_{ij}(\boldsymbol{p}, \boldsymbol{q}, z) = \frac{\varphi_d^2}{4\pi^2} \int \mathrm{d}^2 p' \int \mathrm{d}^2 q' W_{ij}(\boldsymbol{p}', \boldsymbol{q}', 0) \\ \times \exp\left(i\tfrac{1}{2}\varphi_d(|\boldsymbol{q} - \boldsymbol{q}'|^2 - |\boldsymbol{p} - \boldsymbol{p}'|^2)\right). \end{aligned} \tag{2.24}$$

The effect of turbulence is incorporated into this model using the extended Huygens-Fresnel principle [56], in which the field is assumed to acquire a random complex phase

$\psi(\boldsymbol{p},\boldsymbol{p'})$ during propagation from the source point $\boldsymbol{p'}$ to the detector point $\boldsymbol{p}$, i.e.

$$\begin{aligned} W_{ij}(\boldsymbol{p},\boldsymbol{q},z) = \frac{\varphi_d^2}{4\pi^2}\int \mathrm{d}^2p' \int \mathrm{d}^2q' W_{ij}(\boldsymbol{p'},\boldsymbol{q'},0) \\ \times \exp\left(i\tfrac{1}{2}\varphi_d(|\boldsymbol{q}-\boldsymbol{q'}|^2 - |\boldsymbol{p}-\boldsymbol{p'}|^2)\right) \\ \times \left\langle \exp(\psi^*(\boldsymbol{p},\boldsymbol{p'}) + \psi(\boldsymbol{q},\boldsymbol{q'}))\right\rangle . \end{aligned} \tag{2.25}$$

For a Gaussian power spectrum, the complex phase term can be approximated as a quadratic exponential,

$$\left\langle \exp(\psi^*(\boldsymbol{p},\boldsymbol{p'}) + \psi(\boldsymbol{q},\boldsymbol{q'}))\right\rangle = \exp\left[-\tfrac{1}{4}\gamma_n(R^2 + \boldsymbol{R}\cdot\boldsymbol{R'} + R'^2)\right], \tag{2.26}$$

where $\boldsymbol{R} = \boldsymbol{q}-\boldsymbol{p}$, $\boldsymbol{R'} = \boldsymbol{q'}-\boldsymbol{p'}$ and $\gamma_n = \frac{4}{3}(.55C_n^2k^2z)^{6/5}$ [57]. Using this quadratic approximation allows us to develop an analytic model for atmospheric propagation of our beams.

It is to be noted that the effects of turbulence and diffraction on the propagated beam are distinct. Turbulence randomizes the phase of the beam, decreasing the spatial correlations on propagation; diffraction introduces a deterministic phase on propagation.

The integration of Eq. (2.25) is lengthy but may be done analytically. We choose to evaluate it in terms of the variables $\boldsymbol{R}$, $\boldsymbol{R'}$, $\boldsymbol{\rho} = \frac{1}{2}(\boldsymbol{q}+\boldsymbol{p})$ and $\boldsymbol{\rho'} = \frac{1}{2}(\boldsymbol{q'}+\boldsymbol{p'})$, i.e.

$$\begin{aligned} W_{ij}(\boldsymbol{R},\boldsymbol{\rho},z) = \frac{\varphi_d^2 A_W}{4\pi^2}\int \mathrm{d}^2R' \int \mathrm{d}^2\rho' A_W W_{ij}^{(s)}(\boldsymbol{R},\boldsymbol{\rho},0) \\ \times \exp(-\gamma_{\rho'}\rho'^2 - \tfrac{1}{4}\gamma_{R'}R'^2 + i\varphi_0\,\boldsymbol{\rho'}\cdot\boldsymbol{R'}) \\ \times \exp\left(i\varphi_d(\boldsymbol{\rho}-\boldsymbol{\rho'})\cdot(\boldsymbol{R}-\boldsymbol{R'})\right) \\ \times \ \exp(-\tfrac{1}{4}\gamma_n(R^2 + \boldsymbol{R}\cdot\boldsymbol{R'} + R'^2)), \end{aligned} \tag{2.27}$$

where $\gamma_{\rho'} = \gamma'_{1'}$, $\varphi_0 = \gamma''_{1'}$ and $\gamma_{R'} = \gamma'_{1'} + \gamma_{2'}$, where $\gamma_{\alpha'}$ are the values before propagation.

In this way, the result for the propagated cross-spectral density is given as

$$W_{ij} = A_W W_{ij}^{(s)} e^{-\gamma_\rho \rho^2 - \frac{1}{4}\gamma_R R^2 + i\varphi_z \boldsymbol{\rho}\cdot\boldsymbol{R}}, \tag{2.28}$$

$$W_{ij}^{(s)} = C_i^* C_j \sum_{\ell=0}^{m} c_{ij\ell} \gamma_s^\ell P_i^{m_i-\ell} Q_j^{m_j-\ell}, \tag{2.29}$$

$$Q_i = \gamma_1(z) q_{\pm_i} + \tfrac{1}{2}\gamma_2(z) R_{\pm_i}, \tag{2.30}$$

$$P_i = Q_i^\dagger = \gamma_1^*(z) p_{\mp_i} - \tfrac{1}{2}\gamma_2^*(z) R_{\mp_i}, \tag{2.31}$$

but with new definitions of the γ_α parameters.

These results should be compared with Eqs. (2.11)-(2.14); we are able to write the cross-spectral density matrix on propagation in free space or in turbulence in the same form as the cross-spectral density in the source plane. The parameters of the propagated model are

$$\gamma_1(z) = -i\varphi_d \frac{\gamma_v}{\Gamma}, \tag{2.32}$$

$$\gamma_2(z) = \left[(\varphi_d+\varphi_0)\frac{\varphi_d}{\gamma_{\rho'}} - \tfrac{1}{2}\gamma_n + i\varphi_d\right]\frac{\gamma_v}{\Gamma} - i\gamma_{1'}\frac{\varphi_d}{\gamma_{\rho'}}, \tag{2.33}$$

$$\gamma_s = \gamma_{s'} + \frac{|\gamma_{1'}^2|}{\gamma_{\rho'}} - \frac{|\gamma_v|^2}{\Gamma}, \tag{2.34}$$

where

$$\Gamma = \gamma_{R'} + \gamma_n + (\varphi_d + \varphi_0)^2/\gamma_{\rho'} \tag{2.35}$$

and

$$\gamma_v = \gamma_{1'} + \gamma_{2'} + i\gamma_{1'}(\varphi_d+\varphi_0)/\gamma_{\rho'}\ . \tag{2.36}$$

The last parameter γ_s is a sum of terms arrived at by reducing a binomial expansion after each integration. The above parameters can be used for quite general cases, including propagation through multiple distinct layers of turbulence, but for our initial

model with $\gamma_{1'} = \gamma_{\rho'} - i\varphi_0$ and $\gamma_{s'} = \gamma_{2'} = \gamma_R - \gamma_{\rho'}$ the parameters simplify to

$$\gamma_1 = \gamma_{1'}\frac{\gamma_d}{\Gamma} - i\varphi_d\frac{\gamma_o}{\Gamma}, \tag{2.37}$$

$$\gamma_s = \gamma_{2'}\frac{\gamma_d}{\Gamma} + \gamma_o\frac{\gamma_n}{\Gamma}, \tag{2.38}$$

$$\gamma_2 = \gamma_s - i\gamma_1\frac{3\gamma_n}{2\varphi_d}, \tag{2.39}$$

$$\tag{2.40}$$

where $\gamma_d = \varphi_d^2/\gamma_{\rho'}$ while $\gamma_o = \gamma_{2'} + |\gamma_{1'}^2|/\gamma_{1'}'$. Just as in the initial cross section, γ_1 and γ_s still describe a beam spreading in the same way as a simple beam wander, with

$$\sigma_\lambda^2 = \sigma_{\lambda'}^2 + \frac{\gamma_n}{\varphi_d^2}, \tag{2.41}$$

but now γ_2 is a complex parameter reflecting tilt of the beam that leads to the beam wander.

Unlike in the model of the beam cross section the Gaussian parameters (with the exception of γ_ρ) do not follow as simply from γ_1 and γ_2, with $\gamma_\rho = \gamma_1'$ but now $\varphi_z = -\gamma_1'' - \gamma_2''$ instead of just $-\gamma_1''$ and more than the other parameters $\gamma_R = \gamma_1' + \gamma_s + 3\varphi_d(\varphi_d + \varphi_0)\gamma_n/(\gamma_1'\Gamma) + \frac{3}{4}\gamma_n^2/\Gamma$ no longer fits the mold of our beam wander model. However these relatively small corrections to these Gaussian parameters do not affect the topology determined by the three polynomial γ parameters with which we are concerned.

2.5 Topological changes with propagation

We are now interested in analyzing the behavior of the singularities of $\overline{\mathbf{W}}_{\boldsymbol{a}}^{(s)}$ on propagation through turbulence. So far, we have considered singularities as points in a transverse plane, with the propagation distance z as a parameter of the problem. We may also consider the full evolution of the singularities in three-dimensional space, in which case the singularities are lines that can potentially branch or combine together.

We will focus on this case, where we are looking at the topological structures in three-dimensional space and how those structures depend on various parameters of the system.

It is to be noted that $\overline{\mathbf{W}}_{\boldsymbol{a}}^{(s)}$ is itself a projection of the full cross-spectral density matrix, and the full matrix will have singularities on a higher-dimensional manifold. Our choice of $\boldsymbol{a}$ and $\boldsymbol{p}$ dictates the projection, and the behavior of the singularities will depend on those choices.

2.5.1 Stable projections

In our model, we find that the polarization singularities are stable for larger values of $|\boldsymbol{p}|$, with no significant topological changes (creation or annihilation on propagation), whereas at smaller $|\boldsymbol{p}|$ the number of singular points within a cross section is not conserved with z. When N_s is stable, the singular points rotate and move as the values of the γ parameters change the locations of the zeros of Eq. (2.18); an example is shown in Fig. 2.2.

This general observation might suggest that we should choose an observation point extremely far from the beam axis. In practice, however, the position of the observation point is limited to lie within the finite size of the detector aperture, so some creation/annihilation events are expected. These events, however, happen in pairs of equal and opposite index, so the net topological index will typically be unchanged. Even if singularities do not annihilate, they may wander out of the detector aperture and be effectively lost. Nevertheless we will see that, even with these possibilities, projections of beams with stable topology within a field of view can be found that are similar to that in Fig. 2.2 when there is a balance of the tendency to gain spatial coherence with propagation and lose spatial coherence due to turbulence.

On propagation, the number of singularities in the cross-section of the projection changes through creation or annihilation of pairs of singularities with opposite indices, typically lemons ($n = 1/2$) with stars ($n = -1/2$), and as noted singularities can

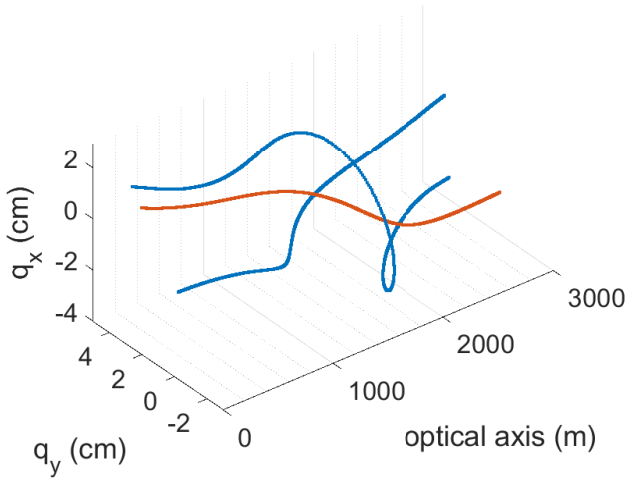

Figure 2.2: Example of a stable trajectory of singularities on propagation. The blue lines represent right-handed circular polarization and the orange line represents left-handed circular polarization. This beam is propagated with turbulence strength $C_n^2 = 10^{-14}$ m$^{-2/3}$. The beam uses $\boldsymbol{t} = (1\ 0)$, $\boldsymbol{C} = (0.01\ \ -1)$ and $\gamma_{1'} = \gamma_{2'} = 0.5$ cm^{-2}. This is projected onto $\boldsymbol{p} = (1\ \ 0)$ cm and a polarization with the major axis 3 times the minor axis and oriented at 30°.

effectively 'disappear' by moving far from the optical axis or 'appear' by moving closer to it from a distant transverse point. An illustration of these effects is shown in Fig. 2.3. As seen in the figure and in other examples we have tested, this appearance and disappearance of singularities also happens in pairs so that these decreases or increases can only affect the topological index of the beam when the singularities are near the aperture boundary, which occurs only over a small range of z values.

Figure 2.3 also shows that multiple creation and annihilation events can arise in the propagation of the beam through turbulence. In the three-dimensional view (q_x, q_y, z), the pairs of singularities that are created or annihilated are seen as a single line connected in a '$\cup$' or '$\cap$' shape. Blue is used to illustrate right-hand circular polarization and orange illustrates left-hand circular polarization. Strikingly, in Fig. 2.3, we see that the topological index remains unchanged on propagation but the handedness of the center singularity flips from right-handed to left-handed. The evolution of the top panel of the figure can be described as follows. We begin

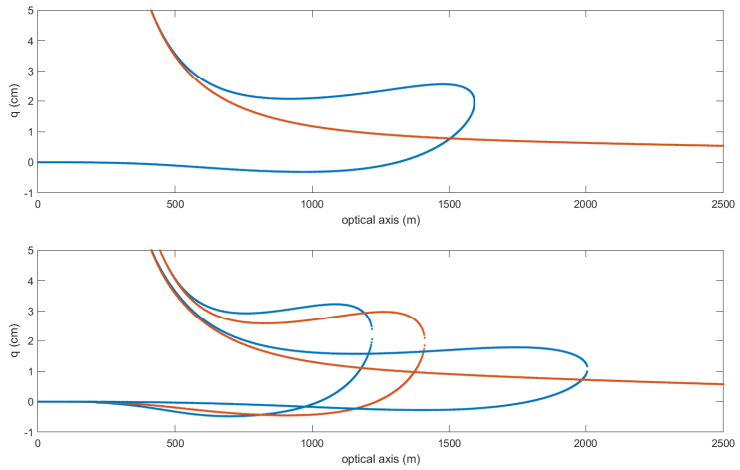

Figure 2.3: Flattened trajectories of polarization singularities along propagation. These lines are three dimensional curves flattened along $\hat{y}$, not a cross-section. The blue lines represent right-handed circular polarization and the orange lines represent left-handed circular polarization. The top has $\boldsymbol{t} = (1\ 0)$ and the bottom has $\boldsymbol{t} = (2\ 1)$ while both have reference point $\boldsymbol{p} = (0.2\ \ 0)$ cm, $\gamma_{1'} = (1 + i)$ cm^{-2}, $\gamma_{2'} = 0$, and $C_n^2 = 8 \times 10^{-15}$ m$^{-2/3}$.

with a lemon singularity $n = 1/2$ that has right-handed circular polarization, and then at approximately 500 m a pair of singularities appears from infinity of opposite handedness and equal and opposite topological index. At roughly 1500 m, the original right-handed lemon annihilates with a right-handed star, leaving behind a left-handed lemon in its place.

These changes in the topology within the field of view along propagation depend not only on the turbulence and initial beam parameters but also on the projection itself; some of these projections can, with a wide enough field of view, be very stable in not just the total topological index, but also the number of singularities.

In the examples considered, the overall topological structure of the beams (namely, the number of singularities and their topological index, though not their handedness) asymptotically approaches a state very close to the original state in the source plane. This is strikingly reminiscent of the behavior of the degree of polarization of electromagnetic beams on propagation in turbulence, where the degree of polarization increases in free space but returns asymptotically to its original value in turbulence

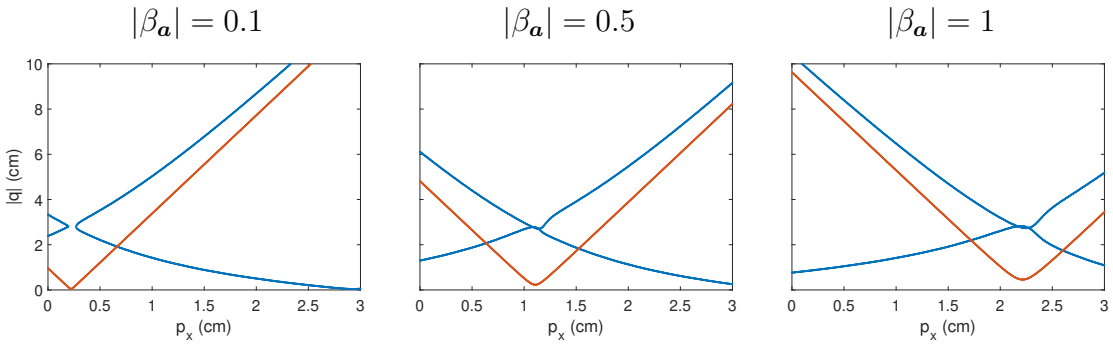

Figure 2.4: The radial position of the polarization singularities as a function of p_x for several values of the ellipse eccentricity $\beta_{\boldsymbol{a}}$. Again, the blue lines represent right-handed circular polarization and the orange lines represent left-handed circular polarization. For these examples, $\boldsymbol{p} = (p_x\, 0)$ at $\Psi_{\boldsymbol{a}} = 30°$ and the eccentricity is determined by $\beta_{\boldsymbol{a}}$. The beam has $\boldsymbol{t} = (1\ \ 0)$, $\gamma_{1'} = \gamma_{2'} = 0.5$ cm^{-2} and $C_n^2 = 10^{-14}$ m$^{-2/3}$. For this beam and turbulence state, each $\boldsymbol{a}$ projected onto has a region of p_x for which the singularities are within a few cm of the optical axis.

[58]. This suggests that the number and/or topological index of partially coherent polarization singularities could be used as information carriers in free-space optical communication systems. However, in many cases these singularities end up migrating away from the optical axis and may lie outside the detector aperture. One way to correct for this is to adjust the projection so that, at the desired propagation distance, the singularities are pushed to within the aperture. An example of this is shown in Fig. 2.4. The radial distance of the singularities of a beam are plotted as a function of p_x for several values of the projection ellipse eccentricity $\beta_{\boldsymbol{a}}$.

It can be seen that the positions of the singularities are strongly affected by the projection choice. A slight change in projection could therefore turn a non-viable information carrying system into a viable one.

2.5.2 Initial coherence interplay with turbulence effects

The propagation of partially coherent fields in turbulence is strongly influenced by two competing factors: the increase of spatial coherence of light on propagation in free space, i.e. the van Cittert-Zernike theorem, and the decrease of spatial coherence due to the random medium. This suggests that the initial state of coherence, i.e. the

coherence area (inverse of the γ_i parameters) of the beam, plays a significant role in its eventual far field properties, including its topological structure. In the near to intermediate regions of propagation, the relative strengths of van Cittert-Zernike increase of coherence and of turbulence decoherence determine if the singularities of the beam move towards or away from the beam center.

We can demonstrate these observations by looking at extreme cases. The first case is when the field is mostly coherent and the turbulence is effectively nonexistent, with $|\gamma_1| \ll \gamma_s$. For larger values of $|\boldsymbol{p}|$, the additional pair of singularities move off towards infinity on propagation, leaving a pure singularity near the beam core, as illustrated in Fig. 2.5(a). The second case is that of $|\gamma_1| \gg \gamma_s$ with nonzero γ_n. For such a beam, the additional pair of polarization singularities that are present in addition to the center singularity move closer to the beam center on propagation, making them visible within the detector aperture and changing the total number of singularities measured (though not their net topological index). This is demonstrated in Fig. 2.5(b). In the even more extreme case of initially coherent beams the singularities also approach the center when losing coherence through turbulence resulting in topology similar to our cross sectional model with partial coherence.

The behavior of a beam's topology in the far field, where γ_n terms dominate, is much more stable. For zero turbulence γ_n is always zero and so propagation under those conditions leads to a far field where the topology of $\overline{\mathbf{W}}_{\boldsymbol{ap}}$ approaches that of a coherent beam with a singularity pair moving toward infinity. For very weak turbulence, this is for practical purposes still the case since the range of z values for which γ_n dominates can be thousands of kilometers. However, when

$$z^{11/5} \gg k^{-7/5}[C_n^2]^{-6/5} \,, \tag{2.42}$$

the polynomial parts of the projection, Eqs. (2.30) and (2.31), become dependent on

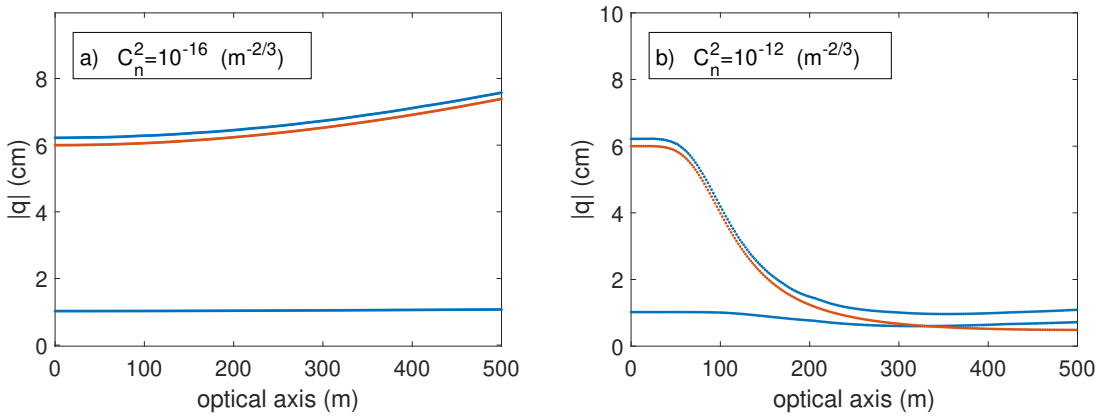

Figure 2.5: Partially coherent polarization singularities of the same beam and projection propagating through a) weak turbulence and b) strong turbulence. The beam has $\boldsymbol{t} = (1\ 0)$, $\gamma_{1'} = 1$ cm^{-2} and $\gamma_{2'} = 0.5$ cm^{-2}. The projection is onto $|\beta_{\boldsymbol{a}}| = 0.5$ at 0° and $\boldsymbol{p} = (1, 0)$ cm. Again, the blue lines represent right-handed circular polarization and the orange lines represent left-handed circular polarization.

$\boldsymbol{R}$ alone. This results in all singularities, even those which went far outside of the field of view or were annihilated, returning towards the center of the beam.

The total number of singularities is therefore not conserved over long propagation distances in turbulence, even if the topological index is conserved. However, the total number of singularities can remain stable over a significant distance, depending on the initial state of coherence and the turbulence strength.

2.5.3 Projections Topology As cross Section of Topology in $(\boldsymbol{p}, \boldsymbol{q}, z)$

As we have seen, when $\overline{\mathbf{W}}$ is projected onto both position $\boldsymbol{p}$ and polarization $\boldsymbol{a}$ it produces a vector field in a three-dimensional space, $\overline{\mathbf{W}}_{\boldsymbol{ap}}(q_x, q_y, z)$, where the singularities are typically lines. The topological index n of a particular singularity line is determined by determining the change of the ellipse orientation around a counterclockwise closed path encircling the line. Lines that connect in annihilation or creation events on propagation will have oppositely signed indices if the index sign is defined assuming the $+z$ direction is used to define the counterclockwise direction for any closed path.

The singularities of $\overline{\mathbf{W}}_{\boldsymbol{ap}}(q_x, q_y, z)$, however, themselves represent a projection of a

higher-dimensional singular manifold that itself is potentially more stable than any individual projection. We may consider less restrictive projections, for example by considering the behavior of $\overline{\mathbf{W}}_{vect}(\boldsymbol{a}, \boldsymbol{p}, \boldsymbol{q}, z) = \boldsymbol{a} \cdot \overline{\mathbf{W}}(\boldsymbol{p}, \boldsymbol{q}, z)$, where $\boldsymbol{a}$ is no longer a constant unit vector, or $\overline{\mathbf{W}}_{\boldsymbol{a}\phi}(p, \boldsymbol{q}, z)$, where the angle of $\boldsymbol{p}$ is fixed but the azimuthal angle is not.

In this section, we get a glimpse of the higher-dimensional singularity structure by considering a collection of projections for a case when N_s is not stable on propagation due to creation and annihilation events.

We have already noted that projections for smaller $|\boldsymbol{p}|$ and smaller $\beta_{\boldsymbol{a}}$ can be unstable, with N_s not constant along the propagation direction. In such a case the singularities tend to stay closer to the beam center, allowing the initial singularities to annihilate each other on propagation and for new singularities to be created after further propagation. The range of projections where this type of volatility in N_s occurs varies with the beam structure itself, increasing as the phase difference $\phi_{C_R} - \phi_{C_L}$ between the components of the beam increases. Such a volatile region of projections can occur for all values of turbulence strength C_n^2, and even in the absence of turbulence, though higher values will cause changes of N_s through annihilation and creation to occur over smaller ranges of z.

In Fig. 2.6, we illustrate the evolution of the projection $\overline{\mathbf{W}}_{\boldsymbol{a}\phi}(p, \boldsymbol{q}, z)$ in three-dimensional space as the value of $p = |\boldsymbol{p}|$ is changed. For small values of p, the singularities completely annihilate for a significant propagation distance and eventually a new pair is created. As p increases, the propagation region over which the singularities are absent grows smaller, and eventually we reach a critical p value for which no annihilation occurs at all. This demonstrates that the singular manifold was never truly absent from our cross-spectral density matrix, only that we missed it with our particular choice of projection. These results suggest that the higher-dimensional singular manifold is more stable than any of its individual projections. Just as we saw

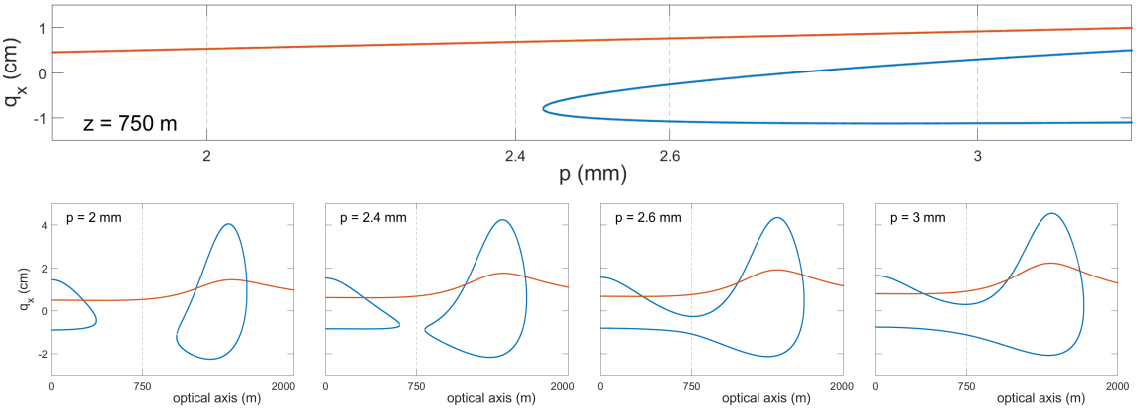

Figure 2.6: The partially polarized singularities of the propagated beams are shown in lines of blue, where the beam has right handed circular polarization and orange where the beam has left circular polarization. These lines are three dimensional curves flattened in $\hat{y}$ of q rather than a cross section. The beam has $\boldsymbol{t} = (1\ 0)$, $\gamma_{1'} = \gamma_{2'} = 1$ cm^{-2} and $C_n^2 = 10^{-14}$ m$^{-2/3}$projected onto $\boldsymbol{a}$ such that $\beta_{\boldsymbol{a}}\beta_C = -5\ m^{-1}$

in Fig. 2.4 that singularities can be constrained to a particular field of view through an appropriate choice of projection, we see that creation and annihilation events can also be suppressed with an appropriate projection.

The higher-dimensional singularity may itself serve as a means to convey information in free space optical communication, though it will require more significant analysis and study, as there is no obvious way to define a topological index n or a total number of singularities N_s for the singular structure of the full cross-spectral density matrix.

2.6 Conclusion

In our previous work, we used a beam wander model to study the types of polarization singularities that can arise in a partially coherent vector field in the source plane and investigated how those singularities depend on source coherence [47]. In this paper, we have expanded this beam wander model of $\overline{\mathbf{W}}$ to include propagation of the cross-spectral density matrix both in free space and in atmospheric turbulence, with a particular interest in the evolution of polarization singularities on propagation.

We focused on those singularities that arise from projecting $\overline{\mathbf{W}}$ onto a single fixed

observation point and polarization state, which results in polarization singularities that are mathematically similar to polarization singularities in a coherent vector field. The net topological index of these beams takes on a discrete half-integer value, as in the coherent case, and suggests that these singularities might be used as robust information carriers in free space optical communications. In general, there is no guarantee that the topological index and the number N_s of polarization singularities will be conserved for a single projection, but we have shown that the stability of these quantities can be improved by an appropriate modification of the projected state.

In this paper, we focused on vector beam propagation through a single region of homogeneous turbulence. However, we have shown that $\overline{\mathbf{W}}$ can be written in the same general mathematical form in the source plane and in the detector plane; see Eqs. (2.11)-(2.14) and (2.28)-(2.31). Therefore, propagation through multiple turbulence layers with different statistics could be modeled by multiple propagation steps and the appropriate changes in the inverse γ widths.

The combination of vector beam singularities with partial coherence involves significant mathematical and theoretical complexity, but it provides another avenue to create new methods of free space communication.

Funding

Air Force Office of Scientific Research [United States] (FA9550-21-1-0171); Office of Naval Research, MURI (N00014-20-1-2558).

Disclosures

The authors declare no conflicts of interest.

CHAPTER 3: A SCALAR POTENTIAL FOR REPRESENTING THE TOPOLOGY OF ELECTROMAGNETIC BEAMS

abstract

It was established by Green and Wolf in 1953 that an electromagnetic wave can be characterized by a complex scalar potential, including its energy and momentum densities. In this paper, we show that for electromagnetic beams this scalar potential can be used to fully describe the beam's topology. We further demonstrate that this scalar potential can be used to characterize a partially coherent vector beam, and introduce a set of scalar Stokes-like parameters for this purpose.

3.1 Introduction

In 1953, Green and Wolf published the paper "A scalar representation of electromagnetic fields," which demonstrated that any electromagnetic wave propagating in free space can be represented exactly by a complex scalar wavefield [59]. Their paper, which is widely regarded as a classic of diffraction theory [60], serves as a broad justification for using scalar waves in electromagnetic theory, and also demonstrates how an energy and momentum density can be defined for such a scalar wave. Wolf followed up this work with a second paper in 1959, which showed how the scalar representation can be employed to introduce a new model of energy transport [61].

Fruitful ideas in physics are often worth revisiting, especially when other developments have the potential to put the ideas in a new context. In this case, the Green-Wolf scalar representation takes on new interest since the recognition that wavefields can possess topological singularities, leading to the extensive field known as *singular optics* [3, 2, 37]. The first exploration of such singularities was done by Nye

and Berry, and they studied phase singularities of scalar wavefields, where the typical form is a line of zero intensity in three-dimensional space around which the phase has a circulating or helical structure, now known as an optical vortex [38]. Nearly a decade later, Nye [44] characterized the singularities of monochromatic paraxial electromagnetic waves, finding that the typical singularities in three-dimensional space are C-lines (lines of circular polarization with undefined polarization ellipse orientation), and L-surfaces (surfaces of linear polarization where the handedness of the field is undefined). Nye and Hajnal later showed that one can also define "true" C-lines and L-lines for non-paraxial electromagnetic waves [62]. An additional class of non-typical singularities are locations where the intensity of the electromagnetic field vanishes and the polarization ellipse orientation is also undefined; in a plane, these are referred to as V-points [50].

The singularities of complex scalar fields and vector fields are topologically distinct. In a transverse plane, scalar singularities are points of zero intensity with a phase that has a topological charge of integer value. In contrast, the singularities of a vector field in a transverse plane have a half-integer topological index associated with them and the field does not have to be zero at the singularity point. The existence of a direct mathematical relationship between scalar and vector fields introduced by Green and Wolf naturally raises the question: what are the singularities of the Green-Wolf complex scalar field and how do those singularities relate to the underlying vector field?

In this paper, we attempt to answer these questions, and demonstrate that the Green-Wolf complex scalar representation provides a natural and unified method for talking about a variety of wavefield singularities in paraxial fields. We present examples to highlight our conclusions.

3.2 The Green-Wolf scalar representation

We begin by introducing the Green-Wolf scalar representation, using some modifications that make it easier to apply to wavefield singularities.

In a region free of charges and currents, the electric field $\mathbf{E}(\mathbf{r}, t)$ and the magnetic field $\mathbf{B}(\mathbf{r}, t)$ may both be derived from the vector potential $\mathbf{A}(\mathbf{r}, t)$, which satisfies the free-space wave equation and may be taken to satisfy the divergence condition

$$\nabla \cdot \mathbf{A}(\mathbf{r}, t) = 0, \tag{3.1}$$

which represents the Coulomb gauge of electromagnetics. Let us work in Cartesian (x, y, z) space and assume that the field is propagating into the positive $\hat{\mathbf{z}}$ space; then it is straightforward to show that the vector potential may be written in the form

$$\mathbf{A}(\mathbf{r}, t) = \int_{k_z>0} \left[\mathbf{a}(\mathbf{k}) \cos(\mathbf{k} \cdot \mathbf{r} - kct) + \mathbf{b}(\mathbf{k}) \sin(\mathbf{k} \cdot \mathbf{r} - kct)\right] d^3k, \tag{3.2}$$

where $\mathbf{k}$ represents the vector spatial frequency, k_z is the zth component of k, and c represents the vacuum speed of light. The integral is over the positive half-space of $\mathbf{k}$. The representation of Eq. (3.2) is the decomposition of the vector potential into real vector plane waves of different frequencies and propagation directions. It is to be noted that this representation does not include evanescent waves and therefore is only valid for free-propagating waves.

From the gauge condition (3.1), each plane wave must be transverse, i.e. $\mathbf{a} \cdot \mathbf{k} = 0$ and $\mathbf{b} \cdot \mathbf{k} = 0$. Green and Wolf satisfy this condition by introducing a pair of unit vectors $\mathbf{l}_1$ and $\mathbf{l}_2$,

$$\mathbf{l}_1(\mathbf{k}) = \frac{\mathbf{n} \times \mathbf{k}}{|\mathbf{n} \times \mathbf{k}|}, \tag{3.3}$$

$$\mathbf{l}_2(\mathbf{k}) = \frac{\mathbf{k} \times \mathbf{l}_1}{|\mathbf{k} \times \mathbf{l}_1|}, \tag{3.4}$$

where $\mathbf{n}$ is a fixed unit vector such as $\hat{\mathbf{x}}$, $\hat{\mathbf{y}}$ or $\hat{\mathbf{z}}$. The vectors $\mathbf{a}(\mathbf{k})$ and $\mathbf{b}(\mathbf{k})$ are then decomposed in terms of these unit vectors,

$$\mathbf{a} = a_1\mathbf{l}_1 + a_2\mathbf{l}_2, \tag{3.5}$$

$$\mathbf{b} = b_2\mathbf{l}_1 + b_2\mathbf{l}_2. \tag{3.6}$$

Green and Wolf immediately generated a complex scalar field $V(\mathbf{r}, t)$ associated with this vector potential by creating the complex combinations

$$\alpha = a_1 + ia_2, \tag{3.7}$$

$$\beta = b_1 + ib_2, \tag{3.8}$$

such that

$$V(\mathbf{r}, t) = \int_{k_z>0} \left[\alpha(\mathbf{k})\cos(\mathbf{k}\cdot\mathbf{r} - kct) + \beta(\mathbf{k})\sin(\mathbf{k}\cdot\mathbf{r} - kct)\right] d^3k. \tag{3.9}$$

They observed that the vector potential can always be retrieved at any point from the corresponding complex scalar field by mapping the complex components into their corresponding vector components. Furthermore, the electromagnetic momentum density $\mathbf{g}(\mathbf{r}, t)$ can be determined from the scalar potential by the expression,

$$\mathbf{g}(\mathbf{r}, t) = -\frac{\epsilon_0}{2}\left[\frac{\partial V^*}{\partial t}\nabla V + \frac{\partial V}{\partial t}\nabla V^*\right], \tag{3.10}$$

with the asterisk denoting the complex conjugate.

In optics, it is more common to work with the electric field, which is simply related to the vector potential by the expression

$$\mathbf{E}(\mathbf{r}, t) = -\frac{\partial}{\partial t}\mathbf{A}(\mathbf{r}, t). \tag{3.11}$$

We may then define a pair of new vectors

$$\mathbf{c}(\mathbf{k}) = k\mathbf{b}(\mathbf{k}), \tag{3.12}$$

$$\mathbf{d}(\mathbf{k}) = -k\mathbf{a}(\mathbf{k}), \tag{3.13}$$

and with these vectors the electric field has the form

$$\mathbf{E}(\mathbf{r}, t) = \int_{k_z>0} [\mathbf{c}(\mathbf{k}) \cos(\mathbf{k} \cdot \mathbf{r} - kct) + \mathbf{d}(\mathbf{k}) \sin(\mathbf{k} \cdot \mathbf{r} - kct)] \, d^3k. \tag{3.14}$$

A complex scalar representation $E(\mathbf{r}, t)$ of the electric field is then introduced by the expressions

$$c(\mathbf{k}) = c_1 + ic_2, \tag{3.15}$$

$$d(\mathbf{k}) = d_1 + id_2, \tag{3.16}$$

such that

$$E(\mathbf{r}, t) = \int_{k_z>0} [c(\mathbf{k}) \cos(\mathbf{k} \cdot \mathbf{r} - kct) + d(\mathbf{k}) \sin(\mathbf{k} \cdot \mathbf{r} - kct)] \, d^3k. \tag{3.17}$$

For a monochromatic field, the polarization ellipse of the electric field and the corresponding vector ellipse of the vector potential will have a very simple relation, and $\mathbf{A}$ can be used in place of $\mathbf{E}$, and we will do so when it is convenient. For a general time-dependent field, however, Eq. (3.11) indicates that the fields will not be equivalent.

3.3 Monochromatic beams and their singularities

We are interested in seeing how the topology of singularities in the real vector field are related to the singularities in the complex scalar field.

Let us restrict ourselves to the simplest case: monochromatic paraxial fields, i.e.

beams. In such a case, the fields may be taken to lie fully in the $x-y$ plane to a good approximation, with negligible z-components. There are two natural choices for the basis vectors $\mathbf{l}_1$ and $\mathbf{l}_2$ in this case: the first is to take $\mathbf{l}_1 = \hat{\mathbf{x}}$, which results in $\mathbf{l}_2 = \hat{\mathbf{y}}$. It is to be noted that it is also possible to choose $\mathbf{n}$ in Eqs. (3.3) and (3.4) as $\hat{\mathbf{z}}$, in which case the set of vectors $\mathbf{l}_1$ and $\mathbf{l}_2$ (keeping only transverse components) are azimuthally-variant and possess a singularity at the origin themselves,

$$\mathbf{l}_1 = -\sin\phi\hat{\mathbf{x}} + \cos\phi\hat{\mathbf{y}}, \tag{3.18}$$

$$\mathbf{l}_2 = -\cos\phi\hat{\mathbf{x}} - \sin\phi\hat{\mathbf{y}}. \tag{3.19}$$

We will stick to the fixed $\hat{\mathbf{x}}$, $\hat{\mathbf{y}}$ basis for simplicity, but this freedom of basis choice is noteworthy: although the gauge of $\mathbf{A}$ is fixed, we retain some freedom in defining our fields and potentials through the basis.

In our fixed transverse basis, the total vector field takes on a particularly simple form, as each component can be integrated separately, so that

$$\mathbf{E}(\mathbf{r},t) = \mathbf{C}(\mathbf{r},t) + \mathbf{D}(\mathbf{r},t), \tag{3.20}$$

with

$$\mathbf{C}(\mathbf{r},t) = \int_{k_z>0} [c_1(\mathbf{k})\hat{\mathbf{x}} + c_2(\mathbf{k})\hat{\mathbf{y}}]\cos(\mathbf{k}\cdot\mathbf{r} - kct)d^2k, \tag{3.21}$$

$$\mathbf{D}(\mathbf{r},t) = \int_{k_z>0} [d_1(\mathbf{k})\hat{\mathbf{x}} + d_2(\mathbf{k})\hat{\mathbf{y}}]\sin(\mathbf{k}\cdot\mathbf{r} - kct)d^2k. \tag{3.22}$$

Because we are working with monochromatic fields, it is to be noted that $|\mathbf{k}| = k_0$ is now a constant and the integral is only over the direction of $\mathbf{k}$. To further study the properties of these fields, we express the sine and cosine functions in complex form in

the usual way. We may then write

$$\mathbf{C}(\mathbf{r},t) = \frac{1}{2}\int_{k_z>0} [c_1(\mathbf{k})\hat{\mathbf{x}} + c_2(\mathbf{k})\hat{\mathbf{y}}]\,[\exp[i\Delta] + \exp[-i\Delta]]\,d^2k, \tag{3.23}$$

$$\mathbf{D}(\mathbf{r},t) = -\frac{i}{2}\int_{k_z>0} [d_1(\mathbf{k})\hat{\mathbf{x}} + d_2(\mathbf{k})\hat{\mathbf{y}}]\,[\exp[i\Delta] - \exp[-i\Delta]]\,d^2k, \tag{3.24}$$

where we have written $\Delta = \mathbf{k}\cdot\mathbf{r} - k_0ct$ for brevity. We may then write the electric field in terms of two integrals,

$$\begin{aligned}\mathbf{E}(\mathbf{r},t) = &\frac{1}{2}\int_{k_z>0} [c_1\hat{\mathbf{x}} + c_2\hat{\mathbf{y}} - id_1\hat{\mathbf{x}} - id_2\hat{\mathbf{y}}]\exp[i\Delta]d^2k \\ &+ \frac{1}{2}\int_{k_z>0} [c_1\hat{\mathbf{x}} + c_2\hat{\mathbf{y}} + id_1\hat{\mathbf{x}} + id_2\hat{\mathbf{y}}]\exp[-i\Delta]d^2k.\end{aligned} \tag{3.25}$$

We may define the propagated form of each component of the field as

$$\tilde{c}_i(\mathbf{r}) \equiv \int_{k_z>0} c_i(\mathbf{k})\exp[i\mathbf{k}\cdot\mathbf{r}]d^2k, \tag{3.26}$$

with $i = 1, 2$ and a similar definition for $\tilde{d}_i$. We may then write an expression for the real-valued electric field in the form,

$$\mathbf{E}(\mathbf{r},t) = \mathrm{Re}\left\{\left[\tilde{c}_1\hat{\mathbf{x}} + \tilde{c}_2\hat{\mathbf{y}} - i\tilde{d}_1\hat{\mathbf{x}} - i\tilde{d}_2\hat{\mathbf{y}}\right]\exp[-i\omega t]\right\}, \tag{3.27}$$

where $\omega = k_0c$ and we have suppressed the obvious spatial argument of the components for brevity.

We now focus only on the positive frequency component, i.e. $\exp[-i\omega t]$ with $\omega > 0$, and label the field of this component as $\mathbf{E}_p$. We now rewrite it in terms of the circular polarization basis,

$$\hat{\mathbf{e}}_\pm = \frac{\hat{\mathbf{x}} \pm i\hat{\mathbf{y}}}{\sqrt{2}}, \tag{3.28}$$

where a '+' sign represents left-handed circular polarization. With some effort we

arrive at the result

$$\mathbf{E}_p(\mathbf{r},t) = \frac{1}{2\sqrt{2}}\left\{\left[\tilde{c}_1 - i\tilde{c}_2 - i(\tilde{d}_1 - i\tilde{d}_2)\right]\hat{\mathbf{e}}_+ \right. \\ \left. + \left[\tilde{c}_1 + i\tilde{c}_2 - i(\tilde{d}_1 + i\tilde{d}_2)\right]\hat{\mathbf{e}}_-\right\}\exp[-i\omega t]. \tag{3.29}$$

Turning to the singularities of the vector field, we now see that C-points arise in two distinct circumstances. There will be a left-handed C-point if

$$\tilde{c}_1 + i\tilde{c}_2 - i(\tilde{d}_1 + i\tilde{d}_2) = 0, \tag{3.30}$$

and a right-handed C-point if

$$\tilde{c}_1 - i\tilde{c}_2 - i(\tilde{d}_1 - i\tilde{d}_2) = 0. \tag{3.31}$$

Let us turn to the complex scalar field to see how the singularities compare. Starting from Eq. (3.17), we can follow the same process used to derive Eq. (3.27). We then find that we may write

$$E(\mathbf{r},t) = \frac{1}{2}\left\{\tilde{c}_1 + i\tilde{c}_2 - i(\tilde{d}_1 + i\tilde{d}_2)\right\}\exp[-i\omega t] \\ + \frac{1}{2}\left\{\tilde{c}_1 - i\tilde{c}_2 - i(\tilde{d}_1 - i\tilde{d}_2)\right\}^*\exp[i\omega t]. \tag{3.32}$$

In complex scalar form, the field may be written as two complex monochromatic fields, one with frequency $+\omega$ and one with frequency $-\omega$. On comparison with Eqs. (3.30) and (3.31), we find that zeros of the positive frequency component are the locations of right-hand C-points and zeros of the negative frequency component are the locations of left-hand C-points.

It is important to note that the positive and negative frequency components of the scalar field are no longer complex conjugates of each other and now represent the

different circular components of the field. The two vector components of the field have transformed into different temporal frequencies in the scalar representation.

These results are striking because the topology of scalar singularities, i.e. optical vortices, is distinct from the topology of vector singularities such as C-points. Optical vortices are dislocations in a complex scalar field whose generic forms have integer valued topological charge, $t = \pm 1$, while C-points are disclinations in a real vector field whose generic forms have half-integer valued topological index, $n = \pm 1/2$. Despite these differences, the scalar representation shows that the topologies of the two classes of fields can be directly related.

To better understand the nature of the singularities, let us simplify our expressions to the forms,

$$\mathbf{E}_p(\mathbf{r}, t) = [U_+(\mathbf{r})\hat{\mathbf{e}}_+ + U_-(\mathbf{r})\hat{\mathbf{e}}_-] \exp[-i\omega t], \tag{3.33}$$

and

$$E(\mathbf{r}, t) = U_-(\mathbf{r}) \exp[-i\omega t] + U_+^*(\mathbf{r}) \exp[i\omega t], \tag{3.34}$$

where $U_+(\mathbf{r})$ and $U_-(\mathbf{r})$ represent the complex fields associated with the left-hand circular and right-hand circular components of the electric field, respectively.

Let us assume that there is a local singularity near the origin in a transverse $x - y$ plane, such that

$$U_\alpha(\mathbf{r}) \approx (x + \beta i y), \tag{3.35}$$

where $\alpha = \pm 1$, $\beta = \pm 1$. (The singularity can of course be positioned away from the origin without changing the results which follow.) It has been shown [37, Section 7.5] that the singularity will be a star if $\alpha\beta = +1$ and a lemon if $\alpha\beta = -1$. We can therefore introduce both types of C-points into left-handed or right-handed circular polarization by an appropriate choice of vortex sign.

One interesting consequence of these observations is that it is a straightforward process to construct a paraxial electromagnetic wave with polarization singularities

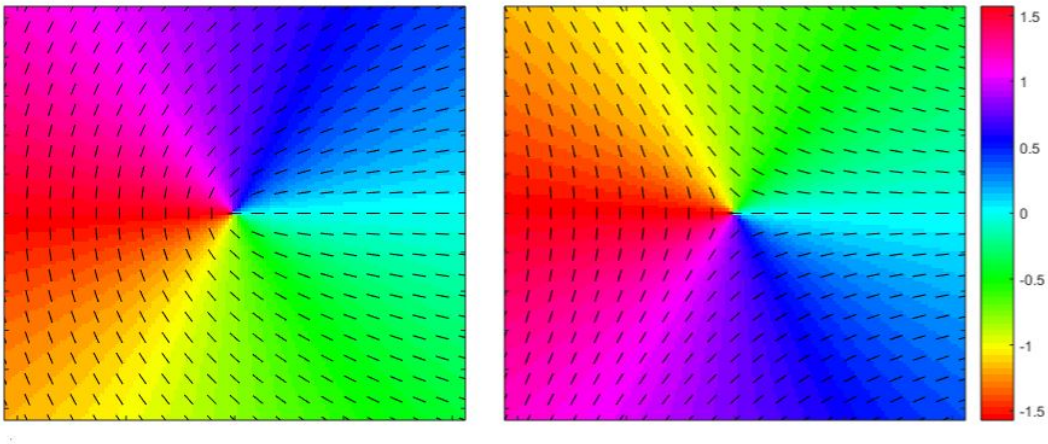

Figure 3.1: This figure shows how the phase of $V_+^{(2)}(\mathbf{r})$ represented by the colors on the diagram from -π to π correspond with double the physical angle of the major axis in the polarization ellipse describing the field at that point.

of any desired type and location by constructing a pair of complex scalar paraxial waves with corresponding vortices and conjugate time dependence.

3.4 Physical properties of the complex scalar

We have seen that, for paraxial electromagnetic beams, the complex scalar potential provides an alternative representation for the singularities of the vector field. However, the scalar potential provides even more information about the state of the vector field, including the complete properties of the polarization ellipse, as we now show.

We work in this case with the scalar representation of the vector potential, having noted that it is directly related to the representation of the electric field for paraxial monochromatic beams. We may then write the scalar representation as

$$V(\mathbf{r},t) = V_-(\mathbf{r})e^{-i\omega t} + V_+^*(\mathbf{r})e^{i\omega t}, \tag{3.36}$$

where $V_-(\mathbf{r})$ and $V_+(\mathbf{r})$ represent the potentials associated with right-handed and left-handed circular polarization, respectively. Let us write each of these potentials

in terms of an amplitude $v_j(\mathbf{r})$ and phase $\phi_j(\mathbf{r})$, with $j = +, -$; we then have

$$V(\mathbf{r}, t) = v_-(\mathbf{r})e^{i[\phi_-(\mathbf{r})-\omega t]} + v_+(\mathbf{r})e^{-i[\phi_+-\omega t]}. \tag{3.37}$$

Let us factor out a phase term,

$$\eta(\mathbf{r}) \equiv [(]\phi_-(\mathbf{r}) - \phi_+(\mathbf{r})]/2, \tag{3.38}$$

and introduce a second phase term

$$\psi(\mathbf{r}, t) \equiv -\frac{\phi_+(\mathbf{r}) + \phi_-(\mathbf{r})}{2} + \omega t. \tag{3.39}$$

With some simple manipulations, Eq. (3.37) takes on the form

$$V(\mathbf{r}, t) = e^{i\eta(\mathbf{r})} \left\{ v_-(\mathbf{r})e^{-i\psi(\mathbf{r},t)} + v_+(\mathbf{r})e^{i\psi(\mathbf{r},t)} \right\}. \tag{3.40}$$

This can be written in terms of cosines and sines as

$$V(\mathbf{r}, t) = e^{i\eta(\mathbf{r})} \left\{ v_M(\mathbf{r}) \cos[\psi(\mathbf{r}, t)] + i v_m(\mathbf{r}) \sin[\psi(\mathbf{r}, t)] \right\}, \tag{3.41}$$

where we have introduced

$$v_M(\mathbf{r}) \equiv v_+(\mathbf{r}) + v_-(\mathbf{r}), \tag{3.42}$$

$$v_m(\mathbf{r}) \equiv v_+(\mathbf{r}) - v_-(\mathbf{r}). \tag{3.43}$$

Equation (3.41) represents a complex field that traces out an ellipse in the complex plane in time, and it is the complex form of the polarization ellipse. All of the parameters of the polarization ellipse can be extracted from this complex expression, and in fact can be done more readily than can be done using the vector field. The

quantities $v_M(\mathbf{r})$ and $v_m(\mathbf{r})$ represent the major and minor axes of the ellipse, and the sign of $v_m(\mathbf{r})$ determines the handedness of the ellipse. The quantity $\eta(\mathbf{r})$ gives the orientation of the polarization ellipse, while $\psi(\mathbf{r}, t)$ gives the current position of the vector field relative to the major axis. The electric field is readily shown to be at located at the same point along the polarization ellipse as the potential at a different time t' where $\psi(\mathbf{r}, t') = \psi(\mathbf{r}, t) + pi/2$.

The special cases of linear and circular polarization, which also represent singularities of the vector field, are easy to determine in this representation. Circular polarization arises when $v_M = \pm v_m$, and linear polarization arises when $v_m = 0$. These same polarization states may also be represented using v_+ and v_-. Circular polarization is the case where either $v_+ = 0$ or $v_- = 0$, and linear polarization arises when $v_+ = v_-$.

3.5 Stokes-like parameters for describing singularities

Because our complex scalar field is explicitly time dependent, it is convenient to instead express its singularities in terms of time-averaged second-order field parameters. These parameters are directly analogous to the Stokes parameters S_0, S_1, S_2, S_3 for vector fields, and allow us to isolate singular points from directly observable properties of the field.

Let us introduce three parameters $V_0^{(2)}(\mathbf{r})$, $V_+^{(2)}(\mathbf{r})$, and $V_3^{(2)}(\mathbf{r})$ as

$$V_0^{(2)}(\mathbf{r}) = \langle V^*(\mathbf{r}, t) V(\mathbf{r}, t) \rangle \tag{3.44}$$

$$V_+^{(2)}(\mathbf{r}) = \langle V(\mathbf{r}, t) V(\mathbf{r}, t) \rangle \tag{3.45}$$

$$V_3^{(2)}(\mathbf{r}) = \langle V^*(\mathbf{r}, t) \tfrac{i}{\omega} \partial_t V(\mathbf{r}, t) \rangle, \tag{3.46}$$

where $\langle \ldots \rangle$ represents the time average. For monochromatic fields, this can be an average over a single cycle or a long time average. We will see that the zeros of these three parameters represent V-points, C-points, and L-lines, respectively.

Let us start with $V_+^{(2)}(\mathbf{r})$. On substitution from Eqs. (3.40) or (3.41) into Eq. (3.44) and taking the time average, we have

$$V_+^{(2)}(\mathbf{r}) = 2e^{2i\eta(\mathbf{r})}v_-(\mathbf{r})v_+(\mathbf{r}) = e^{2i\eta(\mathbf{r})}\frac{v_M^2(\mathbf{r}) - v_m^2(\mathbf{r})}{2}. \tag{3.47}$$

This function vanishes when either $v_+ = 0$ or $v_- = 0$, or equivalently when $v_M = v_m$. These represent points of circular polarization, C-points, and the complex function $V_+^{(2)}(\mathbf{r})$ is analogous to the complex Stokes vector $S_1 + iS_2$, which vanishes at points of circular polarization.

Turning to $V_3^{(2)}(\mathbf{r})$, it is straightforward to show that it takes on the form

$$V_3^{(2)}(\mathbf{r}) = v_-^2(\mathbf{r}) - v_+^2(\mathbf{r}) = -v_m(\mathbf{r})v_M(\mathbf{r}). \tag{3.48}$$

This parameter will vanish when $v_m(\mathbf{r}) = 0$; it therefore characterizes the location of L-lines, which are singularities of the handedness of the polarization ellipse. (Recall that the handedness is given by the sign of v_m, which is undefined when $v_m = 0$.) This choice of $V_3^{(2)}(\mathbf{r})$ was made because $V_-(\mathbf{r})\exp[-i\omega t]$ and $V_+(\mathbf{r})\exp[i\omega t]$ are eigenfunctions of the operator $\frac{i}{\omega}\partial_t$, with eigenvalues of -1 and $+1$. The quantity $V_3^{(2)}(\mathbf{r})$ is therefore analogous to the Stokes parameter S_3, which vanishes when the field is linearly polarized.

Finally, considering $V_0^{(2)}(\mathbf{r})$, we have

$$V_0^{(2)}(\mathbf{r}) = v_+^2(\mathbf{r}) + v_-^2(\mathbf{r}) = \frac{v_M^2(\mathbf{r}) + v_m^2(\mathbf{r})}{2}. \tag{3.49}$$

This parameter clearly represents the total intensity of the beam at point $\mathbf{r}$, and this scalar quantity is thus equivalent to the Stokes parameter $S_0(\mathbf{r})$ of the vector field. Zeros of intensity in a vector field are not typical, but when they occur it is usually at a point in the transverse plane; these are V-points and therefore $V_0^{(2)}(\mathbf{r})$ is a parameter

that isolates the V-points of the field. Such points are also points of undetermined handedness and ellipse orientation, so V-points also satisfy $V_3^{(2)}(\mathbf{r}) = V_+^{(2)}(\mathbf{r}) = 0$.

3.6 Extension to partially polarized vector beams

In his second paper on the scalar potential [61], Wolf noted that his potential could be used to model unpolarized beams, therefore extending his method to beams that possess a degree of randomness to them. Much more recently, Wolf merged the theories of coherence and polarization into a single unified formalism [49, 28], and it is of interest to see whether the scalar potential can be extended to beams with general coherence and polarization properties.

We work in the space-frequency domain of electromagnetic fields, in which case the second-order coherence and polarization properties of a beam can be represented by a cross-spectral density tensor $\mathbf{W}(\mathbf{r}_1, \mathbf{r}_2, \omega)$, whose components are defined as

$$W_{ij}(\mathbf{r}_1, \mathbf{r}_2, \omega) = \langle E_i^*(\mathbf{r}_1, \omega) E_j(\mathbf{r}_2, \omega) \rangle_\omega \,, \tag{3.50}$$

where $i, j = x, y$ and $\langle \ldots \rangle_\omega$ represents an average over an ensemble of monochromatic fields at frequency ω [24]. This tensor characterizes the correlations between different polarization components at two points in space. We may also define the cross-spectral density tensor in terms of circular polarization components, $i, j = +, -$. We will work at a single frequency for the rest of this discussion and suppress further explicit use of ω as an argument.

At a glance, it may seem unlikely that we can fully characterize coherence and polarization with a scalar representation, because our tensor relies on calculating an outer product of vector components, where no such outer product exists for complex fields. Motivated by the previous section of this paper, however, we note that $\mathbf{W}(\mathbf{r}_1, \mathbf{r}_2, \omega)$ may also be fully described by generalized Stokes parameters, introduced

by Korotkova and Wolf [63]. In a circular basis, these parameters have the form,

$$S_0(\mathbf{r}_1, \mathbf{r}_2) = W_{++}(\mathbf{r}_1, \mathbf{r}_2) + W_{--}(\mathbf{r}_1, \mathbf{r}_2), \tag{3.51}$$

$$S_+(\mathbf{r}_1, \mathbf{r}_2) = 2W_{-+}(\mathbf{r}_1, \mathbf{r}_2), \tag{3.52}$$

$$S_3(\mathbf{r}_1, \mathbf{r}_2) = W_{++}(\mathbf{r}_1, \mathbf{r}_2) - W_{--}(\mathbf{r}_1, \mathbf{r}_2), \tag{3.53}$$

and we have used $S_+ = S_1 + iS_2$.

Now let us compare these expressions with our Stokes-like scalar parameters of Section 3.5. We apply the definitions of those Stokes-like parameters and, because our fields are not monochromatic, take both a time average and an ensemble average. Using Eq. (3.36) to define $V(\mathbf{r}, t)$, we end up with the expressions,

$$k^2 V_0^{(2)}(\mathbf{r}_1, \mathbf{r}_2) = k^2 \langle\langle V^*(\mathbf{r}_1, t) V(\mathbf{r}_2, t)\rangle\rangle \tag{3.54}$$

$$= W_{++}(\mathbf{r}_2, \mathbf{r}_1) + W_{--}(\mathbf{r}_1, \mathbf{r}_2), \tag{3.55}$$

$$k^2 V_+^{(2)}(\mathbf{r}_1, \mathbf{r}_2) = k^2 \langle\langle V(\mathbf{r}_1, t) V(\mathbf{r}_2, t)\rangle\rangle \tag{3.56}$$

$$= W_{+-}(\mathbf{r}_1, \mathbf{r}_2) + W_{+-}(\mathbf{r}_2, \mathbf{r}_1), \tag{3.57}$$

$$k^2 V_3^{(2)}(\mathbf{r}_1, \mathbf{r}_2) = k^2 \langle\langle V^*(\mathbf{r}_1, t) \tfrac{i}{\omega} \partial_t V(\mathbf{r}_2, t)\rangle\rangle \tag{3.58}$$

$$= W_{--}(\mathbf{r}_1, \mathbf{r}_2) - W_{++}(\mathbf{r}_2, \mathbf{r}_1). \tag{3.59}$$

We can see that these parameters do not exactly match their vector counterparts, due to the reordering of the arguments of the coefficients. (The factors of k^2 come from Eqs. (3.12) and (3.13) relating the potentials to the fields.) However, we may use the Hermitian property of the cross-spectral density tensor, i.e.

$$W_{ij}(\mathbf{r}_1, \mathbf{r}_2) = W_{ji}^*(\mathbf{r}_2, \mathbf{r}_1), \tag{3.60}$$

to rewrite terms. We find that the Stokes parameters S_0 and S_3 may be written as

$$S_0(\mathbf{r}_1, \mathbf{r}_2) = k^2 \mathrm{Re}\left[V_0^{(2)}(\mathbf{r}_1, \mathbf{r}_2)\right] + ik^2 \mathrm{Im}\left[V_3^{(2)}(\mathbf{r}_1, \mathbf{r}_2)\right], \tag{3.61}$$

$$S_3(\mathbf{r}_1, \mathbf{r}_2) = -k^2 \mathrm{Re}\left[V_3^{(2)}(\mathbf{r}_1, \mathbf{r}_2)\right] + ik^2 \mathrm{Im}\left[V_0^{(2)}(\mathbf{r}_1, \mathbf{r}_2)\right]. \tag{3.62}$$

To do something similar for S_+, we need to introduce an additional parameter $V_-^{(2)}$, defined as

$$V_-^{(2)}(\mathbf{r}_1, \mathbf{r}_2) = \langle\langle V(\mathbf{r}_1, t) \tfrac{i}{\omega} \partial_t V(\mathbf{r}_2, t)\rangle\rangle. \tag{3.63}$$

In terms of elements of the cross-spectral density tensor, it may be written as

$$k^2 V_-^{(2)}(\mathbf{r}_1, \mathbf{r}_2) = W_{+-}(\mathbf{r}_1, \mathbf{r}_2) - W_{+-}(\mathbf{r}_2, \mathbf{r}_1). \tag{3.64}$$

We may then write the Stokes parameter S_+ as

$$S_+(\mathbf{r}_1, \mathbf{r}_2) = k^2 \left[V_+^{(2)}(\mathbf{r}_1, \mathbf{r}_2) + V_-^{(2)}(\mathbf{r}_1, \mathbf{r}_2)\right]. \tag{3.65}$$

We therefore see that the entire state of coherence of the beam at frequency ω is characterized by a single complex correlation potential. The ability to do so comes from separating the orthogonal polarization components into complex fields of positive and negative frequencies, as Eq. (3.34) indicates. The singularities and corresponding topological structure of the partially coherent field can therefore be analyzed using the scalar potential. The singularities of a partially coherent vector beam come in a number of varieties, and we refer to our previous work [47] for a detailed discussion of the possibilities. We note, however, that the simplest class of singularities, known as eta singularities [64], can be written in terms of the generalized Stokes parameter S_0,

$$\eta(\mathbf{r}_1, \mathbf{r}_2) = \frac{S_0(\mathbf{r}_1, \mathbf{r}_2)}{\sqrt{S_0(\mathbf{r}_1, \mathbf{r}_1) S_0(\mathbf{r}_2, \mathbf{r}_2)}}, \tag{3.66}$$

and can therefore also be written in terms of our generalized Stokes-like parameters $V_0^{(2)}$ and $V_3^{(2)}$.

3.7 Dynamic topology of V along L lines

Returning to the coherent case, we note that the complex scalar $V(\mathbf{r}, t)$ also has a phase and therefore has its own topology and topological defects that are distinct from the polarization singularities discussed previously. The topology of these singularities is, however, dynamic, evolving over time, due to the explicit non-separable time dependence of the scalar potential of Eq. (3.36).

Let us briefly consider the nature of these singularities. In a transverse plane, the singularities of a single complex field are typically points; if we add time as a variable, then the singularities will trace out lines as time evolves. Because the field is periodic in time with frequency ω, we expect that these lines will be closed paths or will extend out to infinity (i.e. a closed path that passes through the point at infinity). Looking at Eq. (3.41), which expresses the complex fields in terms of major and minor axes of the polarization ellipse, we can see that the scalar field can only be zero at points where $v_m(\mathbf{r}) = 0$; we therefore expect that the singularities will follow the trajectory of the L-lines of the polarization ellipse.

As a simple example, we consider a monochromatic full Poincaré beam, which possesses all states of polarization in its cross-section [65]. A simple example, in the waist plane $z = 0$, has a complex electric field vector of the form,

$$\mathbf{E}(\mathbf{r}) = E_0 e^{-\rho^2/w_0^2} \left[\hat{\mathbf{e}}_+ + (x + iy)\hat{\mathbf{e}}_-\right], \tag{3.67}$$

where $\rho^2 = x^2 + y^2$, w_0 is the width of the beam, and E_0 is taken real for simplicity. This beam will be linearly polarized at points where the amplitudes of $\hat{\mathbf{e}}_+$ and $\hat{\mathbf{e}}_-$ are equal, i.e. $\rho = 1$.

The corresponding complex potential is of the form,

$$kV(\mathbf{r},t) = E_0 e^{-\rho^2/w_0^2}\left[e^{i\omega t} + (x+iy)e^{-i\omega t}\right]. \tag{3.68}$$

If we separate out the real and imaginary parts of this potential and require them to be equal to zero, we find the conditions

$$-(x+1)\cos(\omega t) = y\sin(\omega t), \tag{3.69}$$

$$y\cos(\omega t) = (x-1)\sin(\omega t). \tag{3.70}$$

If we eliminate time from the equations, we get an equation for the path of the singularity,

$$x^2 + y^2 = 1, \tag{3.71}$$

which is simply the circle of linear polarization $\rho = 1$.

At any snapshot in time one can see the phase singularity has the same topological charge even though other features change as the singular point in phase, or equivalently the direction of the vector field.

A less trivial example,

$$\begin{aligned} V_- &= V_0\left(\frac{r}{w_0}\right)^{|t_-|} e^{it_-\phi} \\ V_+ &= V_0\left(\frac{r}{w_0}\right)^{|t_+|} e^{it_+\phi}\ , \end{aligned} \tag{3.72}$$

where $t_\pm$ can be considered the topological charge of the corresponding component, leads to different numbers of these dynamic singularities as well as, if neither charge is zero, stationary singularities due to v_M and v_m being zero at the origin. Though The stationary points are points of singularity in the orientation of the polarization $\eta(\mathbf{r})$ that also correspond to points of linear polarization(These are only by coincidence

elsewhere called V-points). The more typical C-points are as we have mentioned not singularities in V. Since the dynamic singularities in V occur for the spots along the L-line, $v_m = 0$, where $\frac{1}{2}(t_- + t_+)\phi - \omega t = m\pi$ for any integer m there will be

$$N_{\text{dyn}} = t_- + t_+ \tag{3.73}$$

of these dynamic singularities.

3.8 Conclusions

The scalar potential of Green and Wolf has long been used to justify the description of vector electromagnetic fields by complex scalar fields. With the advent of singular optics, it was of interest to see how the topological defects of vector fields translate into the scalar potential. We have shown that the complex scalar potential allows us to characterize the full behavior of a paraxial monochromatic electromagnetic field and all of its topological defects, and shows how the dislocations of a scalar field may be related to the disclinations of a vector field. Furthermore, we have demonstrated that this scalar representation can even be used for characterizing a partially coherent electromagnetic beam frequency by frequency, including a full derivation of the Stokes parameters.

There are some intuitive advantages to using the scalar representation. The properties of the polarization ellipse, for example, can be easily found from the complex representation as shown in Eq. (3.41), whereas the formulas for these properties in the context of the vector field are significantly less insightful.

We have also seen that the scalar field possesses its own topological features that are directly related to the polarization singularities of the vector field. These time-dependent scalar singularities are reminiscent of, but distinct from, the relativistically invariant Riemann-Silberstein vortices [66] introduced in 2003 and that are connected with a hypothetical photon wave function [67]; it is our hope that the singularities of

the scalar potential will also provoke thoughtful debate.

We note that the bulk of our discussions have focused on paraxial monochromatic fields, even though it has already been shown that the scalar potential can be used for more general cases. It is an open and interesting question whether the singularities of the complex scalar potential have a definite relationship to the vector electromagnetic singularities in this more general case.

Funding

Air Force Office of Scientific Research [United States] (FA9550-21-1-0171); Office of Naval Research, MURI (N00014-20-1-2558).

Disclosures

The authors declare no conflicts of interest.

Conclusions

We are motivated to explore the topologies of beams with a combination of nonuniformly polarized and nonuniform coherence between points within a cross section, as it is a natural extension of polarization and coherence singularities and because both show promise as free space carriers that are robust over propagation through turbulence. As such we looked into the extension of vector vortex beams as Partially polarized vortex beams, finding that they allow for the existence of more intricate topologies than corresponding monochromatic nonuniformly polarized beams or of coherence of the individual components that make them up, in the form of additional singular points.

These partial polarization singularities could be of use in increasing its bandwidth if used as a free space data-carrier in addition to the advantages already motivating the use of partially coherent and nonuniformly polarized vortices. These additional singular points only exist for the topology of field properties that depend on two points, when the cross spectral density of a point with itself is observed, $W(\boldsymbol{r}, \boldsymbol{r}, \omega) = J(\boldsymbol{r}, \omega)$, there are no additional singularities compared to the coherent case. The extra singularities is the result of using a model where the dependence on the distance between two points, $\boldsymbol{R} = \boldsymbol{q} - \boldsymbol{p}$, is not limited to the Gaussian parameters. The Gaussian Schell model is expressed $\boldsymbol{W}(\boldsymbol{p}, \boldsymbol{q}) = \boldsymbol{E}_p^*(\boldsymbol{p}) \otimes \boldsymbol{E}_q(\boldsymbol{q}) \exp[-\gamma_\mu R^2]$, where $\boldsymbol{E}(\boldsymbol{r})$ is coherent, and therefore hides the more typical topology within the original cross section.

Our model, created with a Gaussian beam wander, accomplished this giving extra partially polarized singular point for the projection of the cross spectral density matrix onto a point and polarization. The topology for the phase of the electromag-

netic degree of coherence also has extra singularities but as this number is simply double the singularities in the polarization at a single point this is not a useful in multiplexing the data signal. The total number of partially polarized singularities gives two independent values the number of lemons and starts in equation 1.45. From the standpoint of observation it could be easier to measure directly the number of singularities, $N_{sing} = N_{lemons} + N_{Stars}$ along with the topological index for the entire beam, $n_{total} = \frac{1}{2}(N_{lemons} - N_{Stars})$.

We further find in chapter two that with appropriate choice of projections the 'extra' two point partial polarization singularities, the number of singularities up to the periphery of the beam center is conserved. Though under certain projections the singularities are annihilated only to be created at a much farther distance or move far from the beam center while approaching an opposite index singularity, these can be avoided if the parameters of the vortex beams and turbulence level are known to someone setting up communication with these singularities as the data-carrier. Although we did not write much about the projections onto or in the neighborhood of a point and a polarization orthogonal to the polarized part at that point, which can have more singular points or even singular lines, and did not analyze the effect of propagation on them, knowledge of the beam parameters also allows these projections to be easily avoided so that each input of positively charges (t_+, t_-) corresponds to only one pair of $N_{sings} - n_{beam} = 4\max(m_+, m_-)$.

The multidimensional singularity, for which the projection is just a cross section, was also explored more fully particularly the example with $\boldsymbol{t} = (1 \quad 0)$. This was done not only by exploring the three dimensional projection that leaves just $(\boldsymbol{q}, z)$ as variable coordinates, but also exploring the position of the singularities over changing projection values while holding z constant. With changes in $\Psi_{\boldsymbol{a}}$, where $\boldsymbol{a}$ is the polarization projected onto, the singularities change position along a loop at the cross section of our model with the two left handed circularly polarized C-points

moving closer together with orientations perpendicular to the polarization ellipse of the polarized beam, $J_{pol}(\boldsymbol{p})$, at the coordinate projected onto. The singularities were found to move movement towards and away from the beam center as the shape of that polarization ellipse changes as measured by $|\beta_{\boldsymbol{a}}|$ with the exact function and its minimums determined by the projected position used.

We also discussed how for certain projections the number of singularities can change with propagation through pair annihilation and then creation. When looking at the higher dimensional singularity that the projection is a cross section of we showed that this corresponds to projections that didn't contain the singularities that still existed. This indicates that although the physical meaning of the part of the beam coherent with the field at the projection gives the singularity clear meaning the projection may not be ideal for visualization of the higher dimensional singularity or for observation without more knowledge about which values of $\boldsymbol{p}$ and $\boldsymbol{a}$ make the projection the most visible. One avenue of follow up research that is inspired by this is studying projections onto $\rho = \frac{1}{2}(\boldsymbol{p} + \boldsymbol{q})$ instead $\boldsymbol{p}$ not being able to be limited to only small magnitudes where only one singularity exists as seen in figure 2.4 and the symmetry of the polynomials will allow for a much more stable number of singularities on propagation, and may be more easily observable as well.

While we have concluded that these singularities are persistent over long distances we have not analyzed the feasibility of measuring or setting up an apparatus to switch the topological charges of the circular components both at a high enough frequency to use it as a data carrier. Making a signal requires only the dynamic switching of the topological charges while the elements that structure the coherence of the beam do not necessarily need to be adjustable. For application as a data-carrier the optical elements establishing partial coherence do not have to be variable only those causing variation in the topological index n and $m = \min(m_+, m_-)$, or t_+ and t_-. This variability could eventually be provided by tunable polarization vortex microlasers,

a developing technology, but for the application of free space communication where miniaturization isn't necessary a multitude of setups with two separate adaptive spiral phase plates allows for the production of such a signal. Methodologies for measuring the components of $\overline{\overline{\mathbf{W}}}$ have been devised as early as 2003 [68] and has been realized experimentally [69, 70].

Many of our observations rely to some degree on the class of beams we use to model specific combination of topological indexes. While for the case of the beam cross section the beams initial coherence can be fine tuned through the setup at the source, the propagation through turbulence will create a beam wander like topology just as our more general propagated model with parameters chosen to give coherent or Schell models generated a topology similar to our initial beam wander model on propagation. The model therefore seems very useful for representing the more complex beam while staying in a form that lends itself to analytical analysis.

Finally our utilization of the Green Wolf scalar potential V showed that the topological features of nonuniform polarization in beams could be instead treated as the topology of phase of a complex scalar field. Though the phase that gives the topology of polarization orientation is not directly from V, when constructed for a beam in the manner described it gives the direction of the electric field in $x, y, t)$ whose singularities can be thought of as lines in space time or dynamic singularities moving along the L-lines along time. The L-lines themselves along with c points and other singularities in Ψ are completely defined by the single scalar potential function, but are found by calculating 2nd order parameters of V.

One drawback of this method is the inability to factor a monochromatic field into spatial and temporal parts by using the complex electric field instead of the real electric field. Other than that lack, the simplification that comes from the scalar field can be advantageous for computation and intuition about the beam. The line between phases of the waveform and the angle describing the orientation of the waveform's

polarization ellipse is blurred more than for the vector representation.

It may prove to continue to be useful as it did for representing partially polarized vortex beams as partially coherent complex scalar potential and expanding our parameters to a more general two point statistic for topology in other non-monochromatic beam types.

REFERENCES

[1] G. J. Gbur, *Singular Optics*. CRC Press, 2017.

[2] M. Dennis, K. O'Holleran, and M. Padgett, "Singular optics: Optical vortices and polarization singularities," in *Progress in Optics* (E. Wolf, ed.), vol. 53, (Amsterdam), p. 293, Elsevier, 2009.

[3] M. Soskin and M. Vasnetsov, "Singular optics," in *Progress in Optics* (E. Wolf, ed.), vol. 42, (Amsterdam), p. 219, Elsevier, 2001.

[4] G. Gibson, J. Courtial, M. Padgett, M. Vasnetsov, V. Pas'ko, S. Barnett, and S. Franke-Arnold, "Free-space information transfer using light beams carrying orbital angular momentum," *Opt. Exp.*, vol. 12, pp. 5448–5456, 2004.

[5] J. Wang, J.-Y. Yang, I. Fazal, N. Ahmed, Y. Yan, H. Huang, Y. Ren, Y. Yue, S. Dolinar, M. Tur, and A. Willner, "Terabit free-space data transmission employing orbital angular momentum multiplexing," *Nature Photonics*, vol. 6, pp. 488–496, 2012.

[6] K. Gahagan and G. S. Jr., "Optical vortex trapping of particles," *Opt. Lett.*, vol. 21, pp. 827–829, 1996.

[7] N. Simpson, K. Dholakia, L. Allen, and M. Padgett, "Mechanical equivalence of spin and orbital angular momentum of light: an optical spanner," *Opt. Lett.*, vol. 22, pp. 52–54, 1997.

[8] J. Davis, D. McNamara, D. Cottrell, and J. Campos, "Image processing with the radial Hilbert transform: theory and experiments," *Opt. Lett.*, vol. 25, pp. 99–101, 2000.

[9] S. Fürhapter, A. Jesacher, S. Bernet, and M. Ritsch-Marte, "Spiral phase contrast imaging in microscopy," *Opt. Exp.*, vol. 13, pp. 689–694, 2005.

[10] K. Youngworth and T. Brown, "Focusing of high numerical aperture cylindrical vector beams," *Opt. Exp.*, vol. 7, pp. 77–87, 2000.

[11] R. Dorn, S. Quabis, and G. Leuchs, "Sharper focus for a radially polarized light beam," *Phys. Rev. Lett.*, vol. 91, p. 233901, 2003.

[12] Y. Gu, O. Korotkova, and G. Gbur, "Scintillation of nonuniformly polarized beams in atmospheric turbulence," *Opt. Lett.*, vol. 34, pp. 2261–2263, 2009.

[13] F. Wang, X. Liu, L. Liu, Y. Yuan, and Y. Cai, "Experimental study of the scintillation index of a radially polarized beam with controllable spatial coherence," *Appl. Phys. Lett.*, vol. 103, p. 091102, 2013.

[14] G. Gbur, T. Visser, and E. Wolf, "'Hidden' singularities in partially coherent fields," *J. Opt. A*, vol. 6, pp. S239–S242, 2004.

[15] G. Gbur and T. Visser, "Phase singularities and coherence vortices in linear optical systems," *Opt. Commun.*, vol. 259, pp. 428–435, 2006.

[16] G. Gbur and J. G.A. Swartzlander, "Complete transverse representation of a correlation singularity of a partially coherent field," *J. Opt. Soc. Am. B*, vol. 25, pp. 1422–1429, 2008.

[17] I. Maleev, D. Palacios, A. Marathay, and G. Swartzlander, Jr., "Spatial correlation vortices in partially coherent light: theory," *J. Opt. Soc. Am. B*, vol. 21, pp. 1895–1900, 2004.

[18] W. Wang, Z. Duan, S. Hanson, Y. Miyamoto, and M. Takeda, "Experimental study of coherence vortices: local properties of phase singularities in a spatial coherence function," *Phys. Rev. Lett.*, vol. 96, p. 073902, 2006.

[19] Y. Yang, M. Chen, M. Mazilu, A. Mourka, Y.-D. Liu, and K. Dholakia, "Effect of the radial and azimuthal mode indices of a partially coherent vortex field upon a spatial correlation singularity," *New J. Phys.*, vol. 15, p. 113053, 2013.

[20] C. Stahl and G. Gbur, "Partially coherent vortex beams of arbitrary order," *J. Opt. Soc. Am. A*, vol. 34, pp. 1793–1799, 2017.

[21] C. Felde, A. Chernyshov, G. Bogatyryova, P. Polyanskii, and M. Soskin, "Polarization singularities in partially coherent combined beams," *JETP Lett.*, vol. 88, p. 418, 2008.

[22] M. Soskin and P. Polyanskii, "New polarization singularities of partially coherent light beams," *Proc. SPIE*, vol. 7613, p. 76130G, 2010.

[23] O. Angelsky, A. Mokhun, I. Mokhun, and M. Soskin, "The relationship between topological characteristics of component vortices and polarization singularities," *Opt. Commun.*, vol. 207, pp. 57 – 65, 2002.

[24] E. Wolf, "New theory of partial coherence in the space-frequency domain. part 1: spectra and cross-spectra of steady-state sources," *J. Opt. Soc. Am.*, vol. 72, pp. 343–351, 1982.

[25] C. Stahl and G. Gbur, "Complete representation of a correlation singularity in a partially coherent beam," *Opt. Lett.*, vol. 39, pp. 5985–5988, 2014.

[26] E. Wolf, "Unified theory of coherence and polarization of random electromagnetic beams," *Phys. Lett. A*, vol. 312, pp. 263–267, 2003.

[27] G. Stokes, "On the composition and resolution of streams of polarized light from different sources," *Trans. Camb. Phil. Soc.*, vol. 9, pp. 399–416, 1852.

[28] E. Wolf, *Introduction to the Theory of Coherence and Polarization of Light*. Cambridge: Cambridge University Press, 2007.

[29] E. Wolf, "Can a light beam be considered to be the sum of a completely polarized and a completely unpolarized beam?," *Opt. Lett.*, vol. 33, pp. 642–644, 2008.

[30] S. Raghunathan, H. Schouten, and T. Visser, "Correlation singularities in partially coherent electromagnetic beams," *Opt. Lett.*, vol. 37, pp. 4179–4181, 2012.

[31] S. Raghunathan, H. Schouten, and T. Visser, "Topological reactions of correlation functions in partially coherent electromagnetic beams," *J. Opt. Soc. Am. A*, vol. 30, pp. 582–588, 2013.

[32] M. Marasinghe, M. Premaratne, D. Paganin, and M. Alonso, "Coherence vortices in Mie scattered nonparaxial partially coherent beams," *Opt. Exp.*, vol. 20, pp. 2858–2875, 2012.

[33] Y. Zhang, Y. Cui, F. Wang, and Y. Cai, "Correlation singularities in a partially coherent electromagnetic beam with initially radial polarization," *Opt. Exp.*, vol. 23, pp. 11483–11492, 2015.

[34] F. Gori and M. Santarsiero, "Devising genuine spatial correlation functions," *Opt. Lett.*, vol. 32, pp. 3531–3533, 2007.

[35] J. Tervo, T. Setälä, and A. T. Friberg, "Degree of coherence for electromagnetic fields," *Opt. Exp.*, vol. 11, pp. 1137–1143, 2003.

[36] P. Réfrégier and F. Goudail, "Invariant degrees of coherence of partially polarized light," *Opt. Exp.*, vol. 13, pp. 6051–6060, 2005.

[37] G. Gbur, *Singular Optics*. Boca Raton: CRC Press, 2016.

[38] J. Nye and M. Berry, "Dislocations in wave trains," *Proc. Roy. Soc. A*, vol. 336, pp. 165–190, 1974.

[39] V. Bazhenov, M. Vasnetsov, and M. Soskin, "Laser beams with screw dislocations in their wavefronts," *JETP Lett.*, vol. 52, pp. 429–431, 1990.

[40] L. Allen, M. W. Beijersbergen, R. J. C. Spreeuw, and J. P. Woerdman, "Orbital angular momentum of light and the transformation of laguerre-gaussian laser modes," *Phys. Rev. A*, vol. 45, pp. 8185–8189, Jun 1992.

[41] G. Gibson, J. Courtial, M. J. Padgett, M. Vasnetsov, V. Pas'ko, S. M. Barnett, and S. Franke-Arnold, "Free-space information transfer using light beams carrying orbital angular momentum," *Opt. Express*, vol. 12, pp. 5448–5456, Nov 2004.

[42] M. Malik, M. O'Sullivan, B. Rodenburg, M. Mirhosseini, J. Leach, M. P. J. Lavery, M. J. Padgett, and R. W. Boyd, "Influence of atmospheric turbulence on optical communications using orbital angular momentum for encoding," *Opt. Express*, vol. 20, pp. 13195–13200, Jun 2012.

[43] G. Gbur and R. Tyson, "Vortex beam propagation through atmospheric turbulence and topological charge conservation," *J. Opt. Soc. Am. A*, vol. 25, pp. 225–230, 2008.

[44] J. Nye, "Lines of circular polarization in electromagnetic wave fields," *Proc. Roy. Soc. Lond. A*, vol. 389, pp. 279–290, 1983.

[45] G. Gbur, "Partially coherent beam propagation in atmospheric turbulence [invited]," *J. Opt. Soc. Am. A*, vol. 31, pp. 2038–2045, Sep 2014.

[46] G. Gbur and T. D. Visser, "Phase singularities and coherence vortices in linear optical systems," *Optics Communications*, vol. 259, no. 2, pp. 428–435, 2006.

[47] W. S. Raburn and G. Gbur, "Singularities of partially polarized vortex beams," *Frontiers in Physics*, vol. 8, 2020.

[48] E. Wolf, "New theory of partial coherence in the space–frequency domain. part i: spectra and cross spectra of steady-state sources," *J. Opt. Soc. Am.*, vol. 72, pp. 343–351, Mar 1982.

[49] E. Wolf, "Unified theory of coherence and polarization of random electromagnetic beams," *Physics Letters A*, vol. 312, no. 5, pp. 263–267, 2003.

[50] Ruchi, S. K. Pal, and P. Senthilkumaran, "Generation of v-point polarization singularity lattices," *Opt. Express*, vol. 25, pp. 19326–19331, Aug 2017.

[51] G. Gbur and J. Grover A. Swartzlander, "Complete transverse representation of a correlation singularity of a partially coherent field," *J. Opt. Soc. Am. B*, vol. 25, pp. 1422–1429, Sep 2008.

[52] C. S. D. Stahl and G. Gbur, "Partially coherent vortex beams of arbitrary order," *J. Opt. Soc. Am. A*, vol. 34, pp. 1793–1799, Oct 2017.

[53] Y. Zhang, Y. Cai, and G. Gbur, "Partially coherent vortex beams of arbitrary radial order and a van cittert–zernike theorem for vortices," *Phys. Rev. A*, vol. 101, p. 043812, Apr 2020.

[54] G. A. Swartzlander and R. I. Hernandez-Aranda, "Optical rankine vortex and anomalous circulation of light," *Phys. Rev. Lett.*, vol. 99, p. 163901, Oct 2007.

[55] G. Gbur, "Partially coherent vortex beams," in *Complex Light and Optical Forces XII* (E. J. Galvez, D. L. Andrews, and J. Glückstad, eds.), vol. 10549, p. 1054903, International Society for Optics and Photonics, SPIE, 2018.

[56] R. F. Lutomirski and H. T. Yura, "Propagation of a finite optical beam in an inhomogeneous medium," *Appl. Opt.*, vol. 10, pp. 1652–1658, Jul 1971.

[57] H. T. Yura, "Mutual coherence function of a finite cross section optical beam propagating in a turbulent medium," *Appl. Opt.*, vol. 11, pp. 1399–1406, Jun 1972.

[58] M. Salem, O. Korotkova, A. Dogariu, and E. Wolf, "Polarization changes in partially coherent electromagnetic beams propagating through turbulent atmosphere," *Waves in Random Media*, vol. 14, p. 513, jun 2004.

[59] H. S. Green and E. Wolf, "A scalar representation of electromagnetic fields," *Proceedings of the Physical Society. Section A*, vol. 66, pp. 1129–1137, dec 1953.

[60] K. Oughstun, ed., *Selected papers on Scalar Wave Diffraction*, vol. 51 of *SPIE Milestone Series*, (Bellingham, Washington), SPIE Optical Engineering Press, 1992.

[61] E. Wolf, "A scalar representation of electromagnetic fields: II," *Proceedings of the Physical Society*, vol. 74, pp. 269–280, sep 1959.

[62] J. Nye and J. Hajnal, "The wave structure of monochromatic electromagnetic radiation," *Proc. Roy. Soc. Lond. A*, vol. 409, pp. 21–36, 1987.

[63] O. Korotkova and E. Wolf, "Generalized stokes parameters of random electromagnetic beams," *Opt. Lett.*, vol. 30, pp. 198–200, Jan 2005.

[64] S. B. Raghunathan, H. F. Schouten, and T. D. Visser, "Correlation singularities in partially coherent electromagnetic beams," *Opt. Lett.*, vol. 37, pp. 4179–4181, Oct 2012.

[65] A. M. Beckley, T. G. Brown, and M. A. Alonso, "Full poincaré beams," *Opt. Express*, vol. 18, pp. 10777–10785, May 2010.

[66] I. Bialynicki-Birula and Z. Bialynicka-Birula, "Vortex lines of the electromagnetic field," *Phys. Rev. A*, vol. 67, p. 062114, Jun 2003.

[67] I. Bialynicki-Birula, "On the wave function of the photon," *Acta Phys. Pol. A*, vol. 86, pp. 97–116, 1994.

[68] H. Roychowdhury and E. Wolf, "Determination of the electric cross-spectral density matrix of a random electromagnetic beam," *Optics Communications*, vol. 226, no. 1, pp. 57–60, 2003.

[69] B. Kanseri, S. Rath, and H. C. Kandpal, "Determination of the amplitude and the phase of the elements of electric cross-spectral density matrix by spectral measurements," *Optics Communications*, vol. 282, no. 15, pp. 3059–3062, 2009.

[70] Z. Dong, Z. Huang, Y. Chen, F. Wang, and Y. Cai, "Measuring complex correlation matrix of partially coherent vector light via a generalized hanbury brown–twiss experiment," *Opt. Express*, vol. 28, pp. 20634–20644, Jul 2020.